Atomic Scale Defects: Probing Structure and Function

Felix Hofmann
Department of Engineering Science, University of Oxford, UK.

felix.hofmann@eng.ox.ac.uk

Atomic Scale Crystal Defects

1D

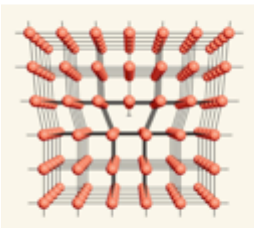

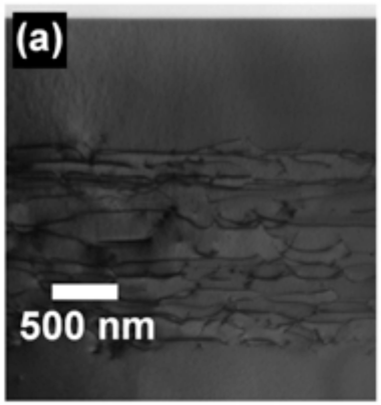

Yang et al., J Cryst Growth (2011)

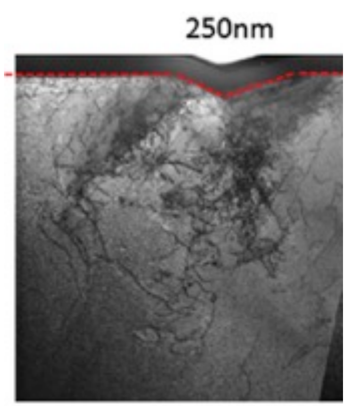

Hardie et al., JNM (2014)

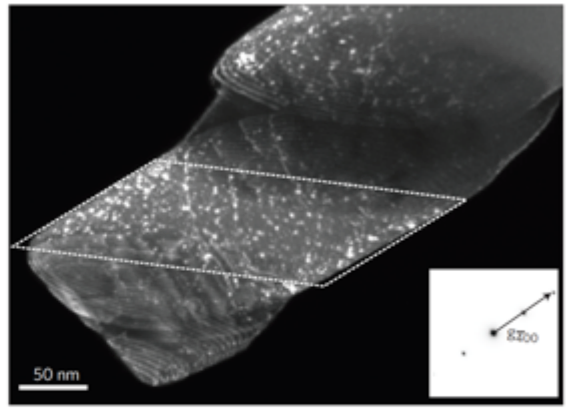

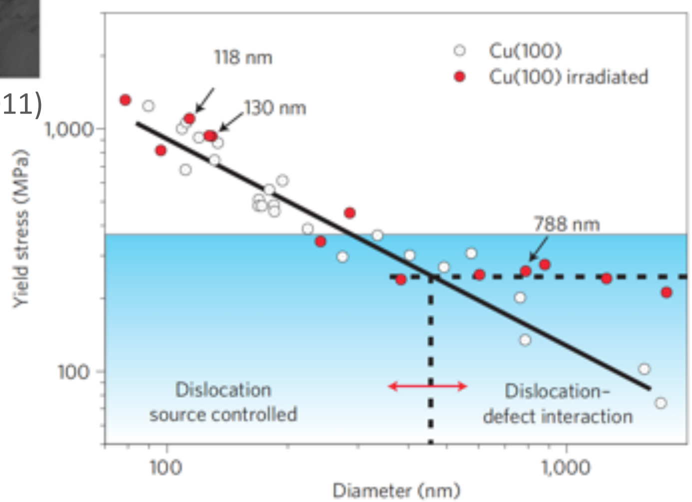

Kiener et al. Nat. Mater. (2011)

3D – 0D

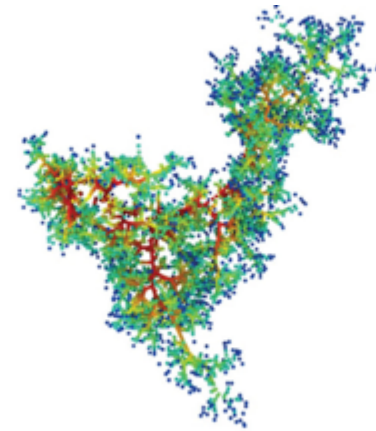

Sand et al., EPL (2013)

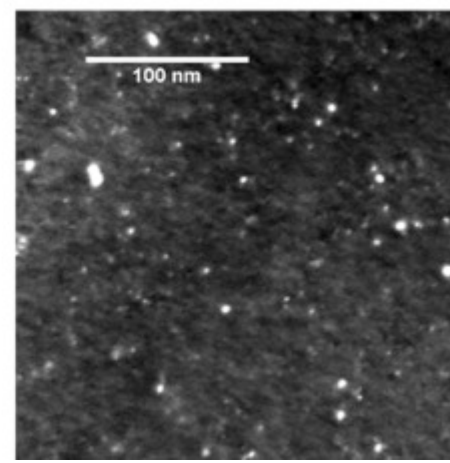

X. Yi et al., arXiv: 1503.02922v1 (2015)

Measuring Defect Strain Fields

Atomic-scale images

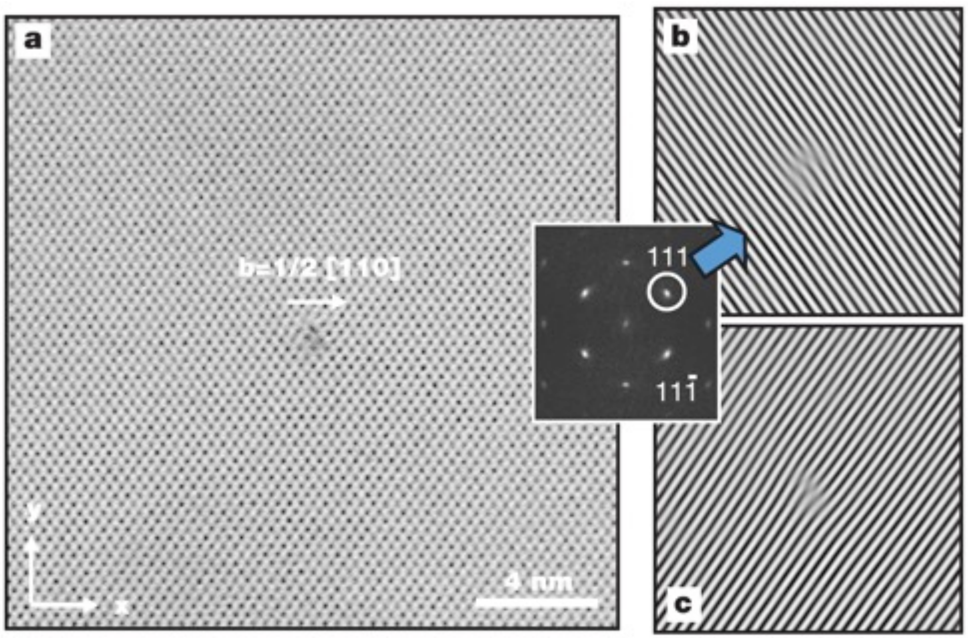

Displacement fields

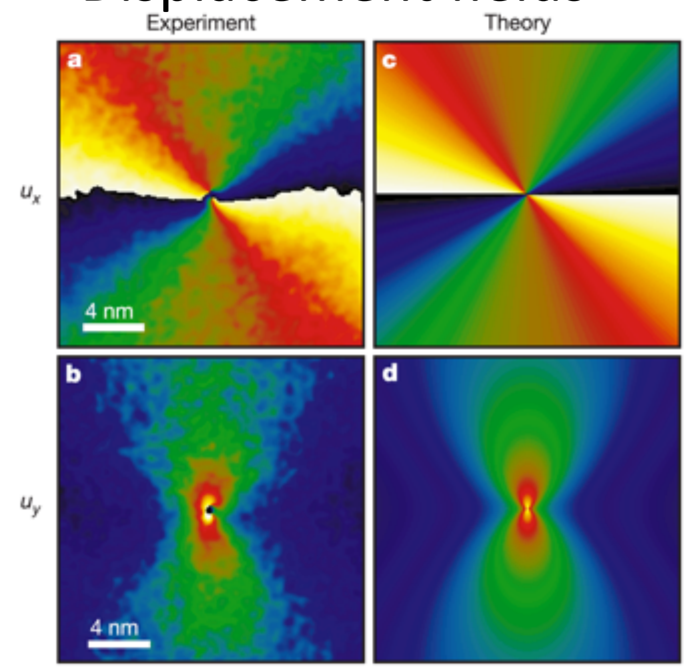

Edge dislocation in silicon, looking down [1-10] direction.

Hytch et al., Nature 423 (2003)

X-ray Imaging of Dislocations

X-ray topograph Etch pits (optical)

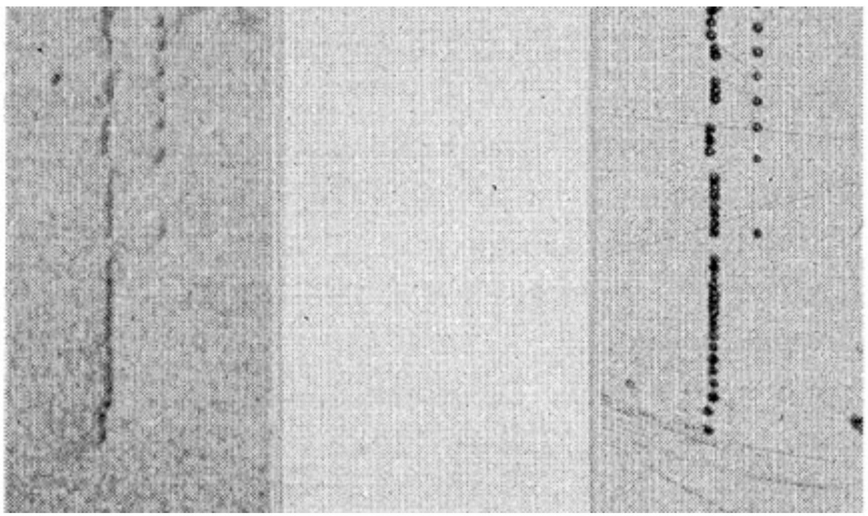

Silicon single crystal. 1st X-ray images of dislocations. Newkirk, Phys. Rev. (1958)

- 3D imaging of dislocations in the bulk
- Dislocation positions
- Low dislocation densities

Topo-Tomography

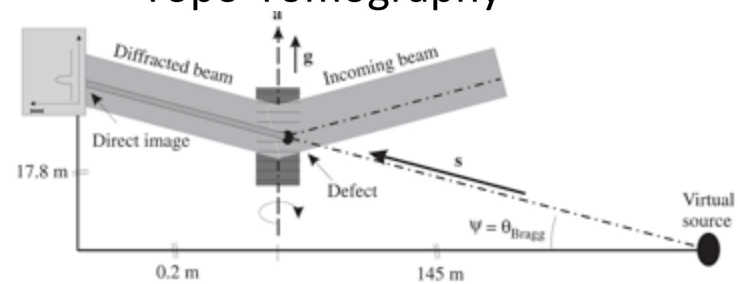

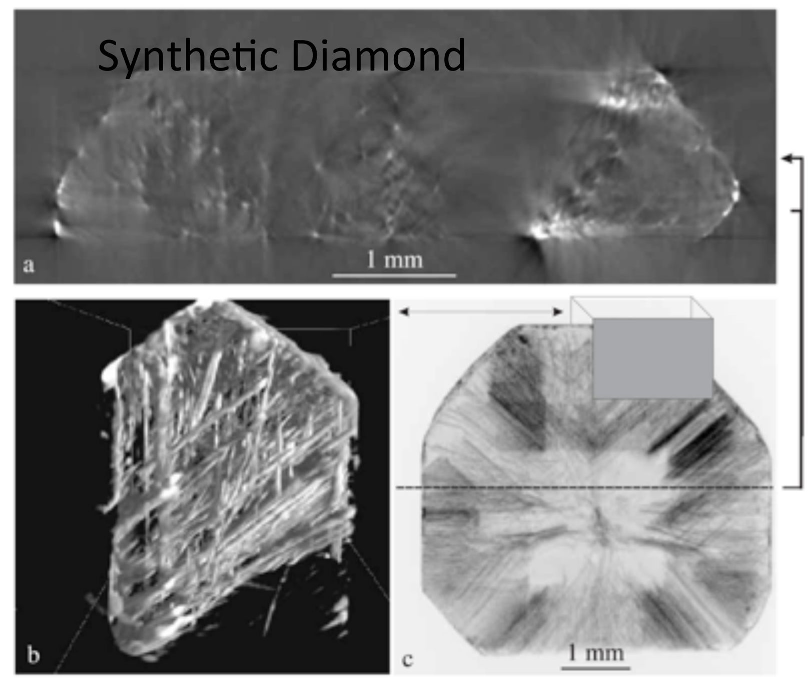

Ludwig et al. J. Appl. Crystallography (2001)

Probing Strains due to an Individual Dislocation

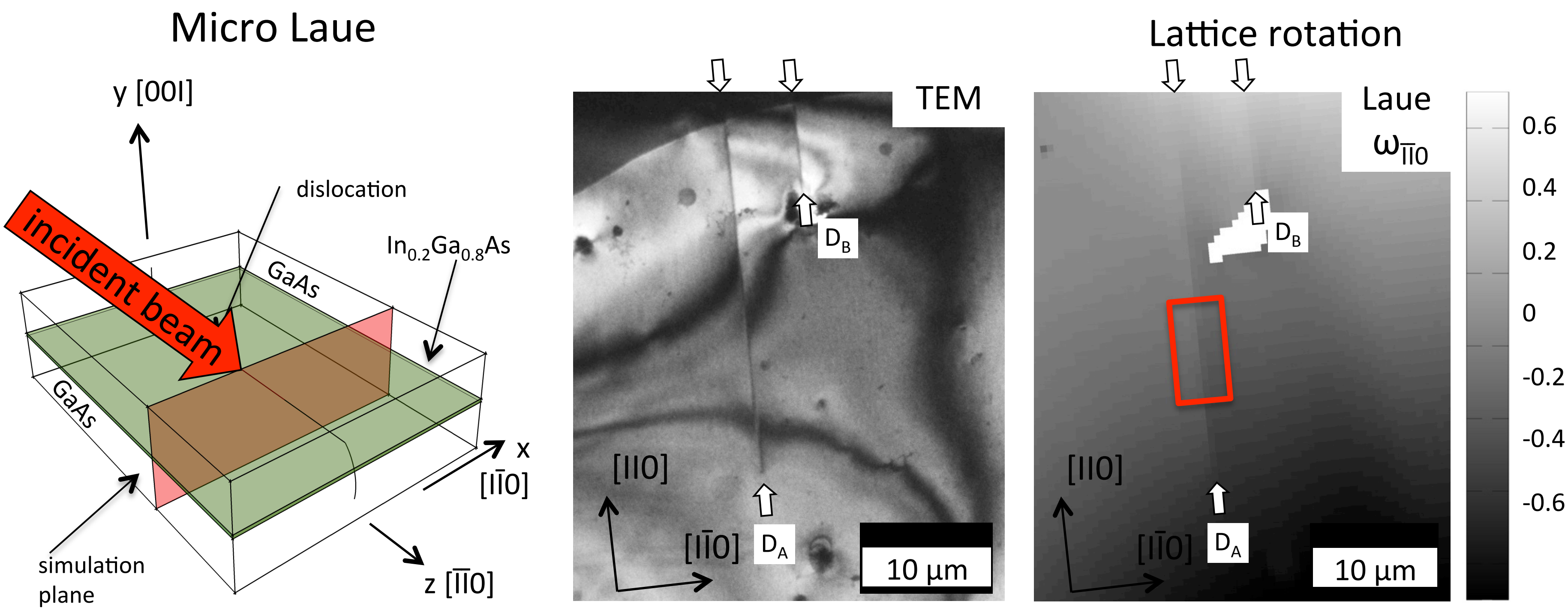

- GaAs-InGaAs multilayer. Misfit dislocations at GaAs-InGaAs interface.
- Easy to see dislocations in TEM.
- Can clearly identify both dislocations in TEM and Laue image

Hofmann et al. Nat. Commun. (2013)

Probing Strains due to an Individual Dislocation

Calculations

Deviatoric elastic strains ($x10^{-6}$)

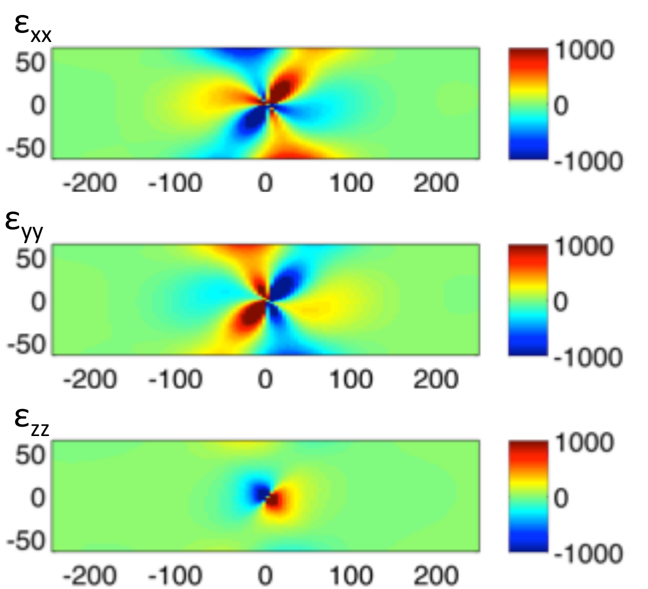

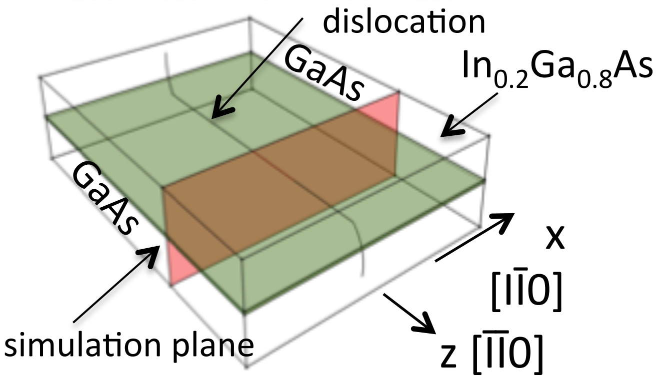

Measurements vs. Predictions

Elastic strains

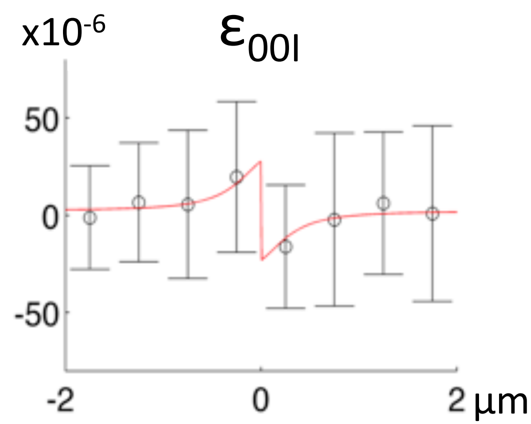

Lattice rotations

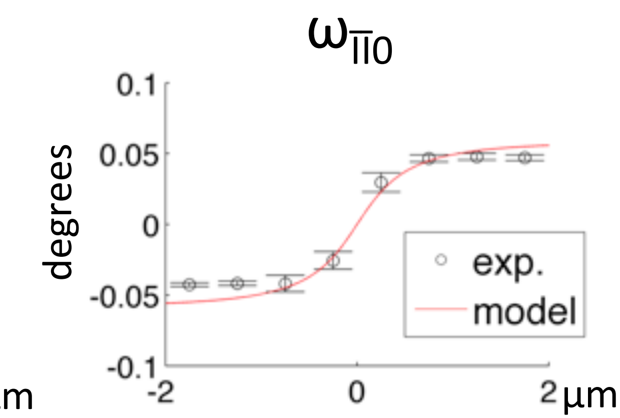

- Anisotropic elasticity modelling.
- “Virtual” diffraction experiment to predict strain and rotation profiles
- Good agreement between prediction and measurement

Hofmann et al. Nat. Commun. (2013)

Outline

- Introduction
- Point Defects

  Irradiation-Induced Defects, Lattice Swelling, Modulus Change, Thermal Transport, DFT, MD, Defect Evolution, Interaction with Dislocations
- Ion-Machining Damage

  Coherent X-ray Diffraction Imaging, Nano-scale Lattice Strains and Crystal Defects
- Conclusions

Tungsten for Plasma-Facing Fusion Armour

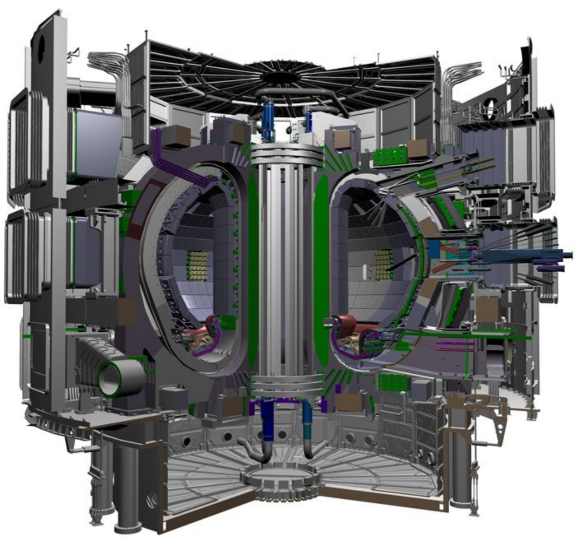

www.iter.org/

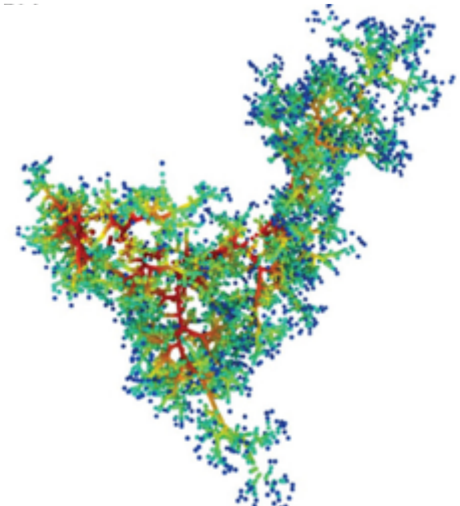

150 keV cascade in W. Colour coded by time red 0fs, blue 200 fs

Sand et al., Europhysics Letters (2013)

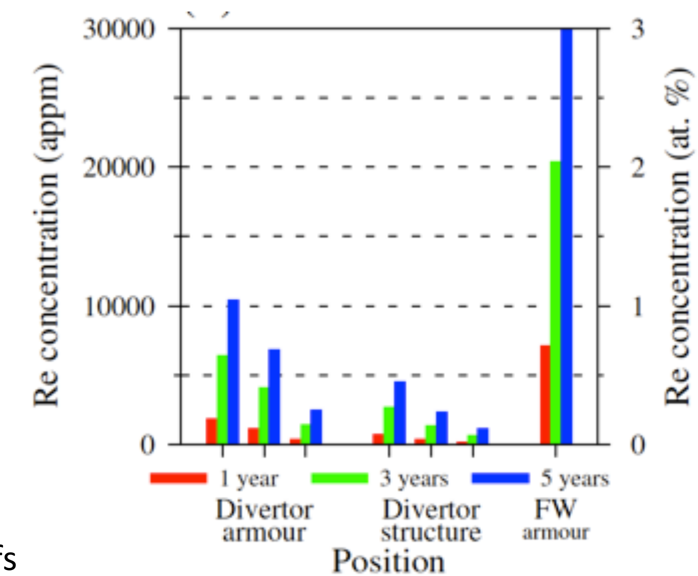

Gilbert et al., Nucl. Fusion (2012)

- High fusion neutron flux[1] (up to ~10^{15} n cm^{-2} s^{-1} per lethargy interval at 14.1 MeV)
  -> collision cascade damage and transmutation alloying
- High operating temperatures (up to ~1500K)
- Intense flux of helium and hydrogen ions and neutrals (up to ~15 MW m^{-1})
  -> high heat loading and implantation-modified structure and properties
  -> **Gas-Defect interaction**

The "Helium Effect" -> Nano-Indentation

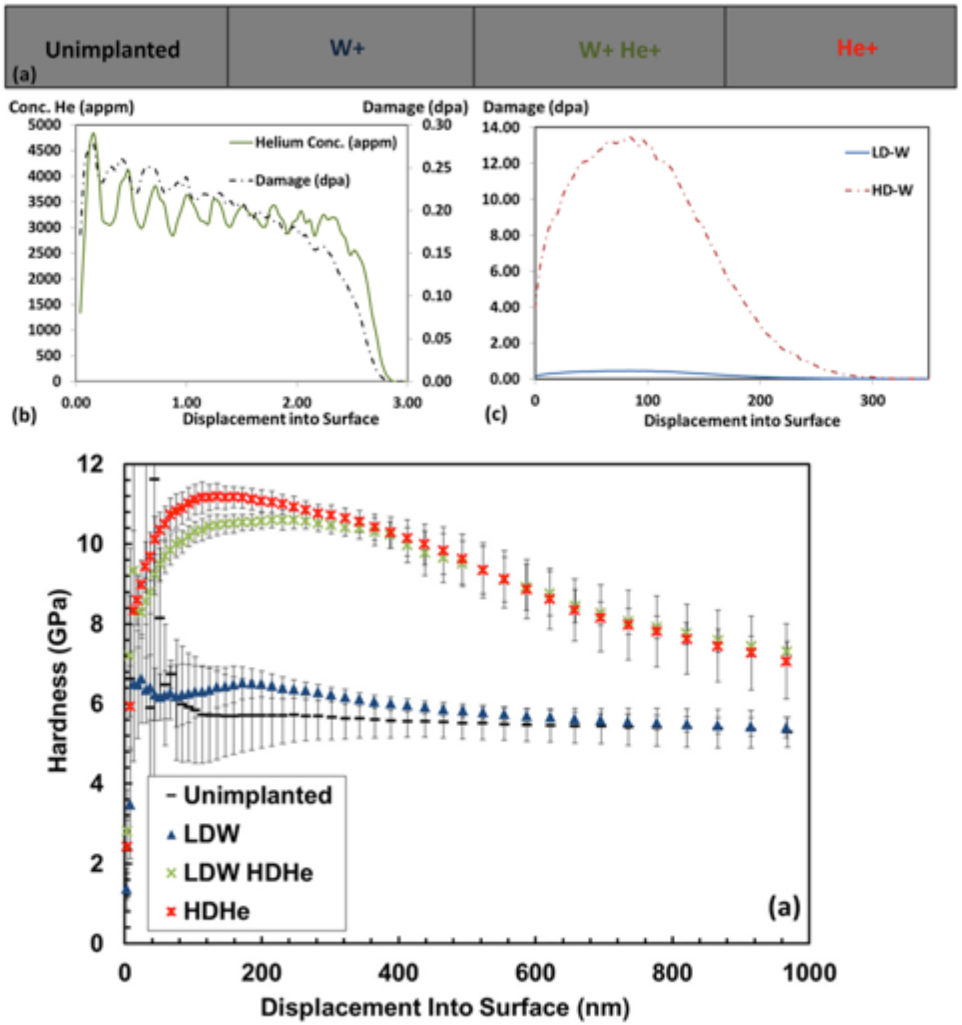

- Ion-implantation of annealed UHP tungsten at 300°C:
  - 3000 appm Helium implantation, multiple energies max. 2 MeV
  - 2 MeV W^+ at 300°C
  - sequential implantation W^+ then He^+
- Small change in hardness due to self ion damage
- Large apparent change in hardness due to helium implantation

Armstrong et al., APL 102 (2013)

Helium-Implanted Tungsten: TEM

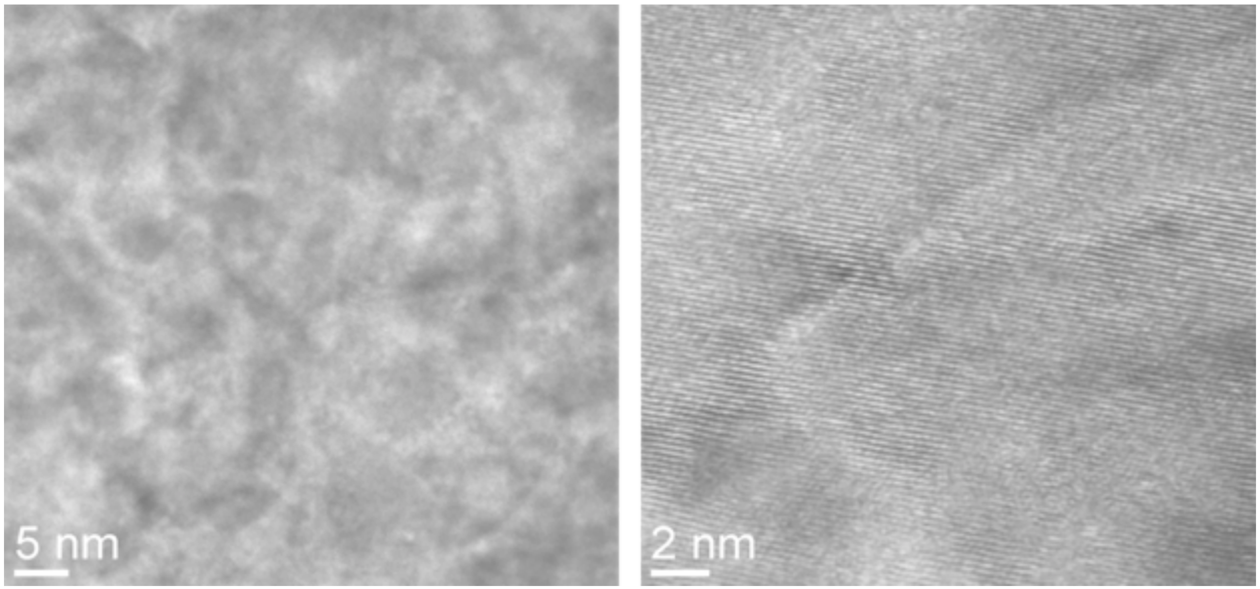

Armstrong et al., APL 102 (2013)

- Pure W + 3000 appm He, 1µm under-focus
- No bubbles or other defects visible
- Storage in vacancies -> Positron annihilation can probe vacancies and vacancy complexes [Debelle JNM 362 (2007) 181-188; Lhuillier JNM 416 2011 13-17].

Quantifying defect numbers is challenging. Lack of spatial resolution.

Samples and Ion-Implantation

Samples

- W and W + Re alloys, plasma arc melted from elemental powders or fully recrystallized rolled material
- No significant texture
- Large 100 to 1000 μm grainsize

Implantation @ NIBC, Surrey

- ~3110 appm He at 300°C
- Fluence - 5.26×10^{16} ions/cm^2
- Multiple energies 0.05-1.8 MeV
- 0.25 dpa displacement damage
- Recoils are predominantly low energy
  - ➢ **Frenkel pair generation dominant damage mechanism**

SRIM implantation profile

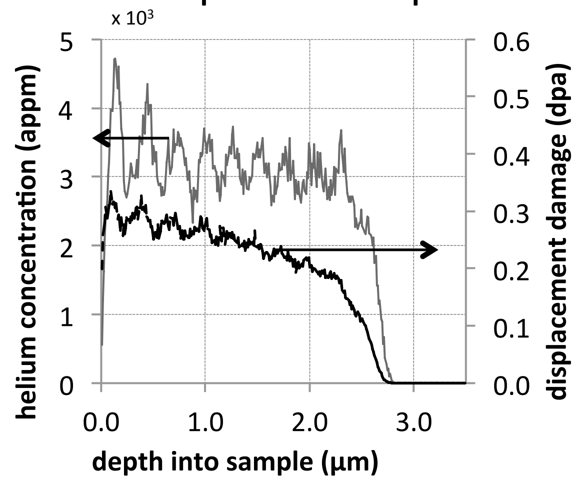

SRIM recoil energies

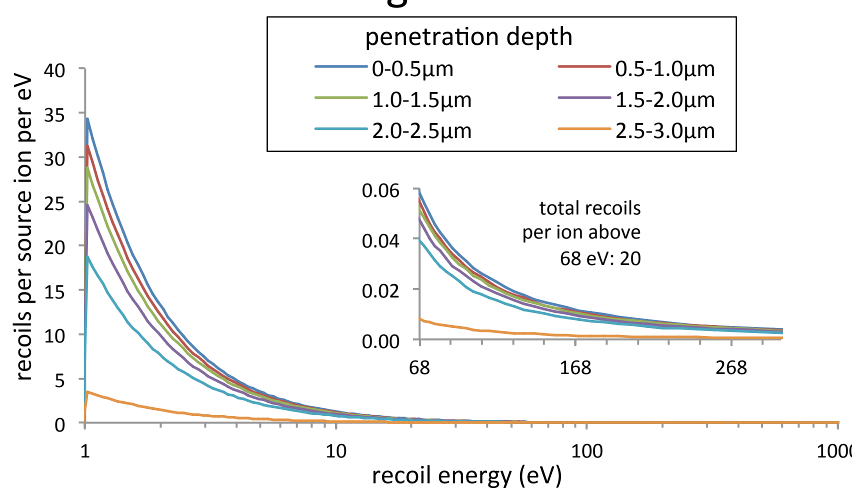

felix.hofmann@eng.ox.ac.uk

Defect-Induced Lattice Swelling

Micro-beam Laue diffraction, 34IDE @ APS

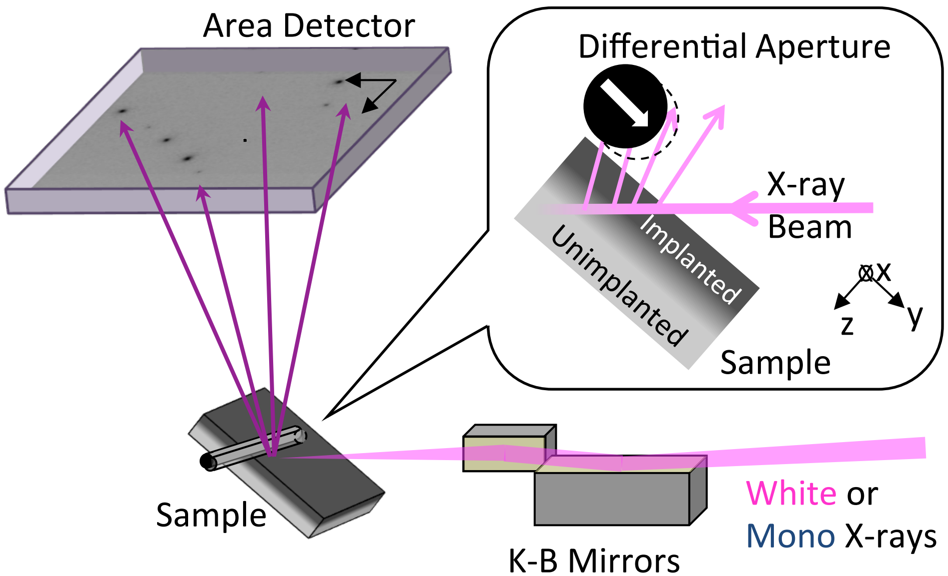

Elastic strain vs. depth in sample

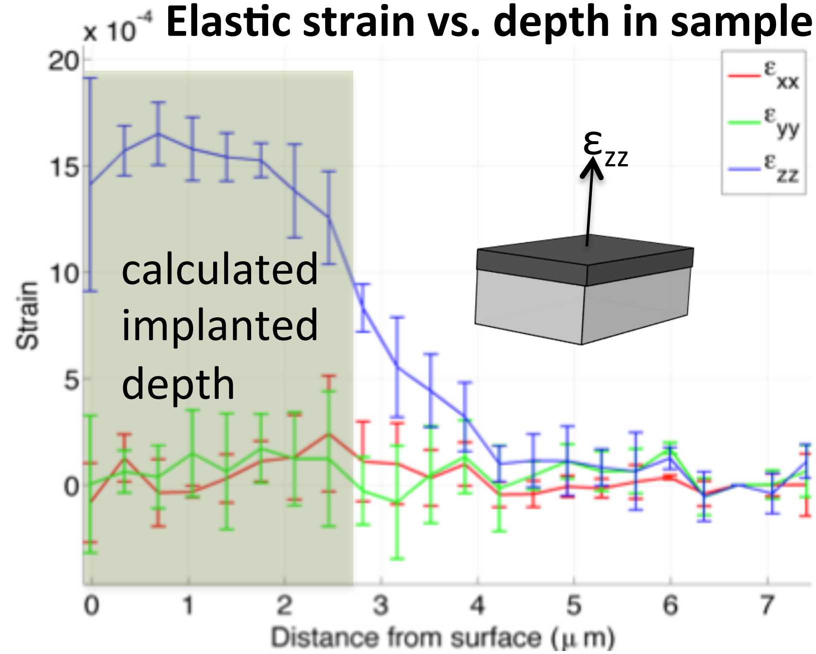

- Differential Aperture X-ray Microscopy (DAXM) -> ~1 µm 3D strain resolution
- In-plane strains (ε_{xx} & ε_{yy}) ~ 0 -> No bubbles upon implantation
- ε_{zz} large in implanted layer -> Lattice swelling $\varepsilon_v = \dfrac{3(1-\nu)}{(1+\nu)}\varepsilon_{zz} = (2620 \pm 200) \times 10^{-6}$

How can this lattice swelling be related to internal defects?

Hofmann et al. Acta Mater. 89 (2015)

DFT Calculations of Relaxation Volume

- Lattice swelling due to implantation-induced defects: $\varepsilon_v = \sum_A n_A \Omega_r^{(A)}$
- Introduce defects within a 4 x 4 x 4 tungsten bcc supercell -> 128 atoms

  Vacancies (V_n), self interstitial atom (SIA), interstitial helium clusters (He_n), helium vacancy clusters (He_nV)
- Boundaries are free to expand -> calculate defect relaxation volumes:

$$\Omega_r(defect) = \Omega(\text{defect}) - \Omega(\text{perfect})$$

111 SIA

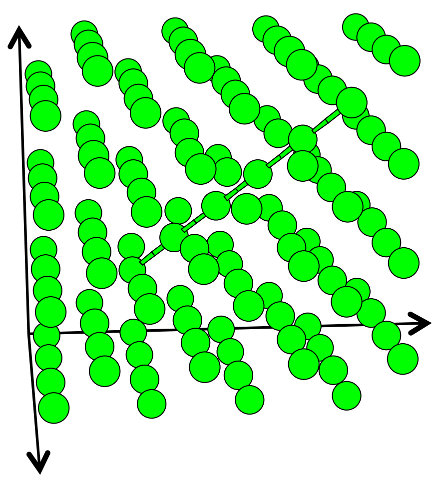

He_2V

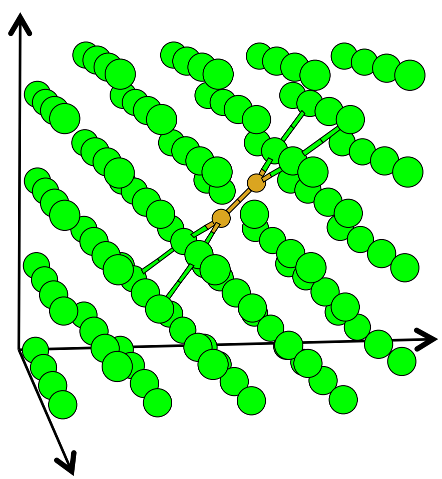

<u>Calculation details:</u>
Perdew-Burke-Ernzerhof electron exchange-correlation functional within generalized gradient approximation. Projector augmented wave (PAW) pseudopotentials implemented in the Vienna Ab-initio Simulation Package (VASP). 400 eV plane wave cutoff energy and 4 x 4 x 4 k-point mesh with 0.15 Å^{-1} spacing. Periodic boundary conditions with expansion in all directions allowed.

Hofmann et al. Acta Mater. 89 (2015)

DFT Calculations of Relaxation Volume

Relaxation volumes for vacancies and self-interstitial

V	V_2 (1NN)	V_2 (2NN)	V_2(3NN)	V_3(1NN(2)+2NN)	<111> SIA	Frenkel
-0.37 -0.34 [1] -0.38 [2]	-0.72 -0.65 [1]	-0.79 -0.74 [1]	-0.76 -0.69 [1]	-1.08	1.68	1.31

Relaxation volumes for interstitial helium clusters

He (tetra)	He (octa)	He_2 (tetra)	He_3 (tetra)	He_4 (tetra)	He_5 (tetra)
0.36 0.33 [3]	0.37 0.34 [3]	0.80	1.16	1.65	2.03

Relaxation volumes for helium - vacancy clusters

HeV (tetra)	HeV (octa)	He_2V (tetra)	He_3V (tetra)	He_4V (tetra)	He_5V (tetra)	He_6V (tetra)
-0.24	-0.23	-0.06	0.14	0.38	0.71	1.09

[1] Kato D, Iwakiri H, Morishita K. Journal of Nuclear Materials 2011;417:1115.
[2] Heinola K, Ahlgren T, Nordlund K, Keinonen J. Physical Review B 2010;82:094102.
[3] Zhou HB, Jin S, Shu XL, Zhang Y, Lu GH, Liu F. EPL (Europhysics Letters) 2011;96:66001.

- **Vacancy relaxation volume: small and negative**
- **SIA relaxation volume: large and positive**
- **Helium-filled vacancy relaxation volume: negative for small n, positive for large n**

Swelling Analysis

- Energetically storage of helium in vacancy clusters is always favourable
  -> assume all helium is stored in the form of He_nV complexes, preventing recombination of Frenkel pairs.

- Swelling modes:
  - Shottky -> accumulation of vacancies in bulk, migration of SIAs to the surface -> would cause some swelling, but little lattice strain
  - Frenkel -> accumulations of helium-filled Frenkel pairs in the bulk -> would cause much more lattice strain -> likely to be the active mechanism here.

- Consider He storage in 3110 appm HeV complexes with 3110 appm SIAs:
  ε_{zz} (HeV + SIA) = 2654×10^{-6}
  - Predict almost twice experimental ε_{zz} strain (1550×10^{-6})

- Consider clustering[1], i.e. 1555 appm He_2V complexes & 1555 appm SIAs:
  ε_{zz} (He_2V + SIA) = 1493×10^{-6}
  - **Good agreement with experimental ε_{zz} strain!**

Hofmann et al. Acta Mater. 89 (2015)

[1] De Backer et al., JNM 429:78 (2012)

Why are SIAs retained?

- SIAs delocalise to form <111> crowdions that are highly mobile (0.05 eV migration energy)[1]
- He-filled vacancies may act as traps for SIAs as shown by recent MD calculations[2, 3]

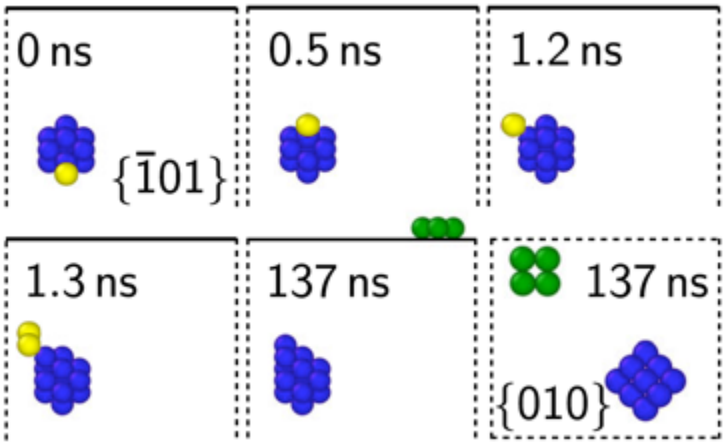

1000 K, atoms participating in vacancy (blue), SIA (yellow), surface adatoms (green)[2]

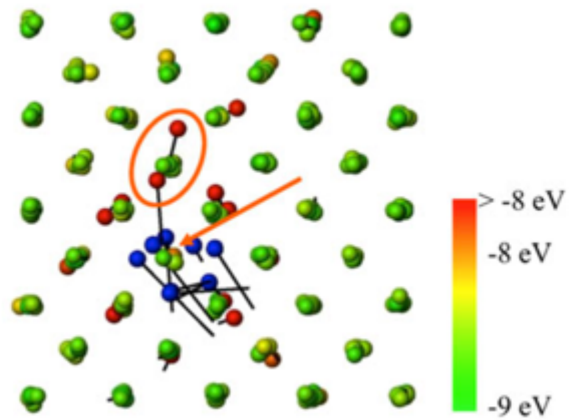

Helium in blue, W atoms coloured by energy. SIA marked by red circle, vacancy by red arrow[3]

[1] Nguyen-Manh et al., Phys. Rev. B 73 (2006) 020101.
[2] Sandoval et al., Phys. Rev. Lett. 114 (2015) 105502.
[3] J. Boisse et al., J. Mater. Res. 29, 20 (2014).

The Effect of Defect Clustering

Large scale atomistic calculations of SIA clusters

- 32 x 32 x 32 atom simulation cell
- Marinica potential for tungsten[1]
- Randomly insert SIAs then relax
- Lateral expansion is constrained

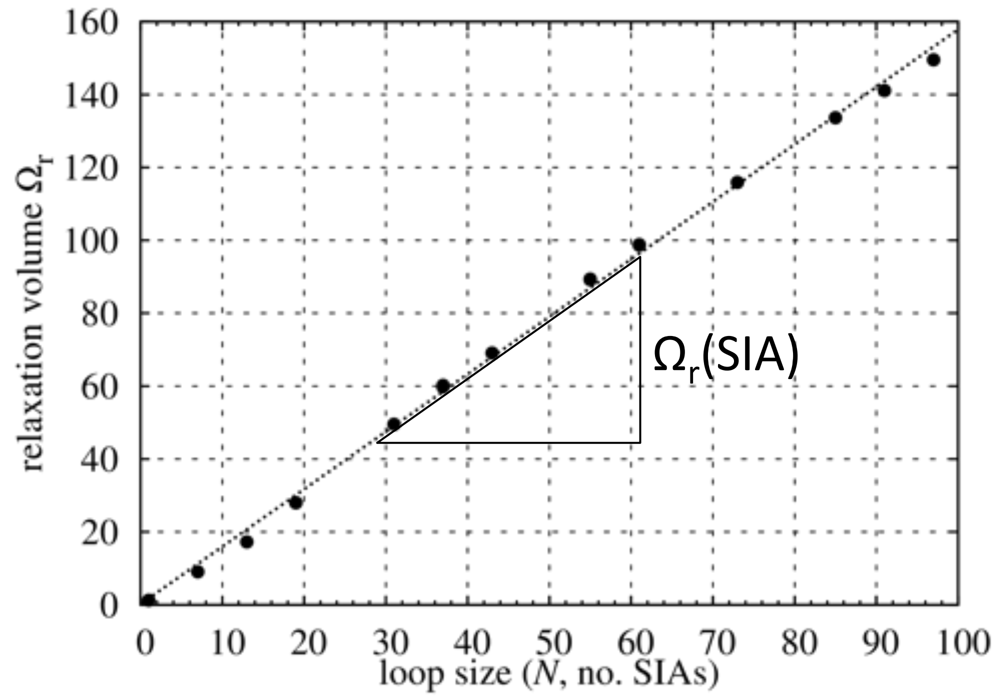

Vacancies

- Immobile at 300°C implantation temperature[2]

SIAs

- <111> crowdions highly mobile at RT[3]
- TEM: clusters < ~60 SIAs
- Relaxation volume scales linearly with number of SIAs in cluster

➢ **Clustering not expected to affect our analysis**

[1]Marinica et al., J. Phys. Cond. Matter 25 (2013)
[2] Rasch et al. Philos. Mag. A 41 (1980)
[3] Nguyen-Manh et al., Phys. Rev. B 73 (2006)

Hofmann et al. Acta Mater. 89 (2015)

Elastic Property Changes

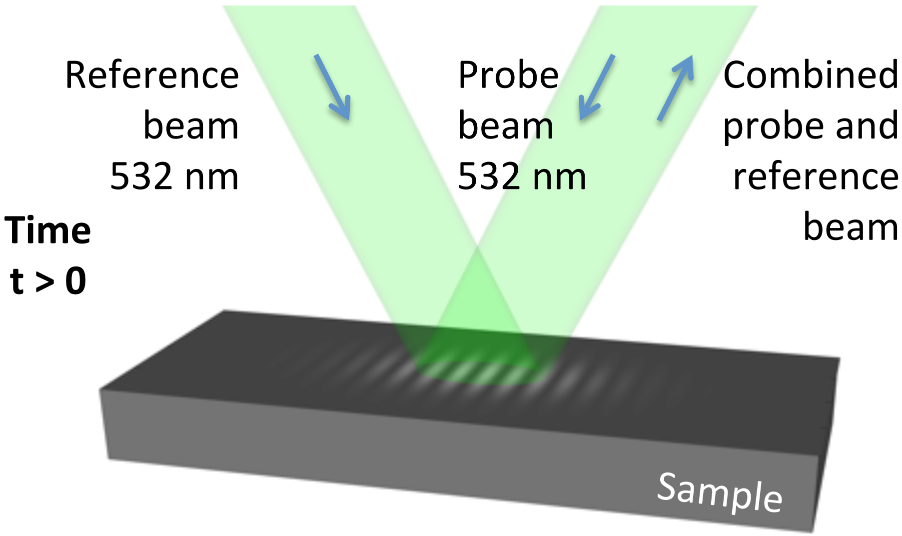

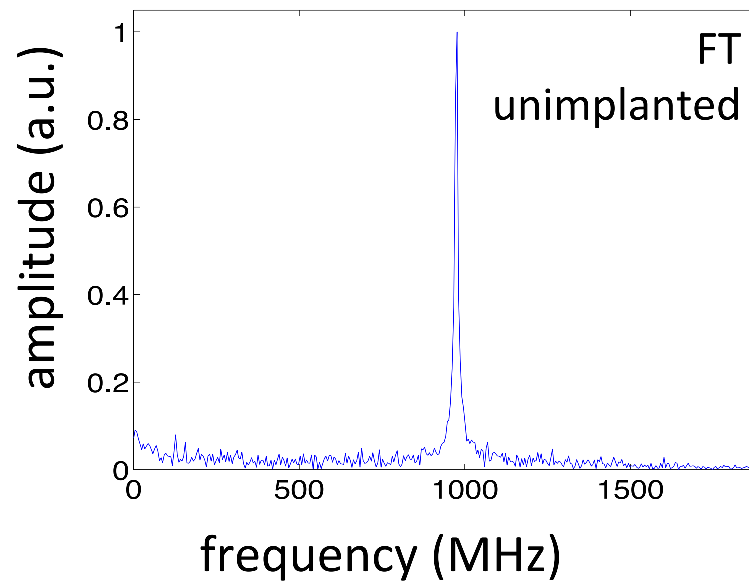

- Transient grating wavelength λ = 2.75 μm
- Surface layer of thickness λ dominates signal
- Rayleigh wave velocities:
  - Unimplanted: 2680 ± 2 ms^{-1}
  - He-implanted: 2621 ± 7 ms^{-1}
    - ➢ **Decrease of c_r by 2.2 %**

$$c_r = f\lambda$$

$$\approx c^* \sqrt{\frac{E}{2(1+\nu)\rho}}$$

shear wave speed

$$c^* = \left(0.874 + 0.196\nu - 0.043\nu^2 - 0.055\nu^3\right)$$

Hofmann et al. Acta Mater. 89 (2015)

Elastic Property Changes

- Implanted material elastic constants (using Voigt approach)

$$C_{ij}^{implanted} = (1-128(n_{SIA}+n_{He_2V}))C_{ij}^{W} + 128n_{SIA}C_{ij}^{SIA} + 128n_{He_2V}C_{ij}^{He_2V}$$

	C_{11} (GPa)	C_{12} (GPa)	C_{44} (GPa)	A	K (GPa)	G (GPa)	E (GPa)	nu
Pure W	522.8	203.5	160.7	1.01	309.9	160.3	410.1	0.279
W + 1555 appm He_2V + 1555 appm SIAs	514.4	208.7	155.5	1.02	310.6	154.5	397.5	0.287

close to isotropic

Modulus ↓ Poisson ratio ↑

- Calculate Rayleigh wave velocity from elastic constants

$$c_r \approx \left(0.874+0.196\nu-0.043\nu^2-0.055\nu^3\right)\sqrt{\frac{E}{2(1+\nu)\rho}}$$

in m/s	calculated		experiments
	Voigt	Reuss	
Perfect W	2667	2667	2679
W + He_2V + SIAs	2622	2618	2621
Change	-1.7%	-1.9%	-2.2%

Hofmann et al. Acta Mater. 89 (2015)

Elastic Property Changes

- <110> W single crystal, implanted with ~3000 appm He at 296 K
- SAW velocity measured as function of angle from <110> direction
- Fit experimental data with calculated SAW velocity for elastically anisotropic material[1]

Measured increase in elastic anisotropy in very good agreement with prediction

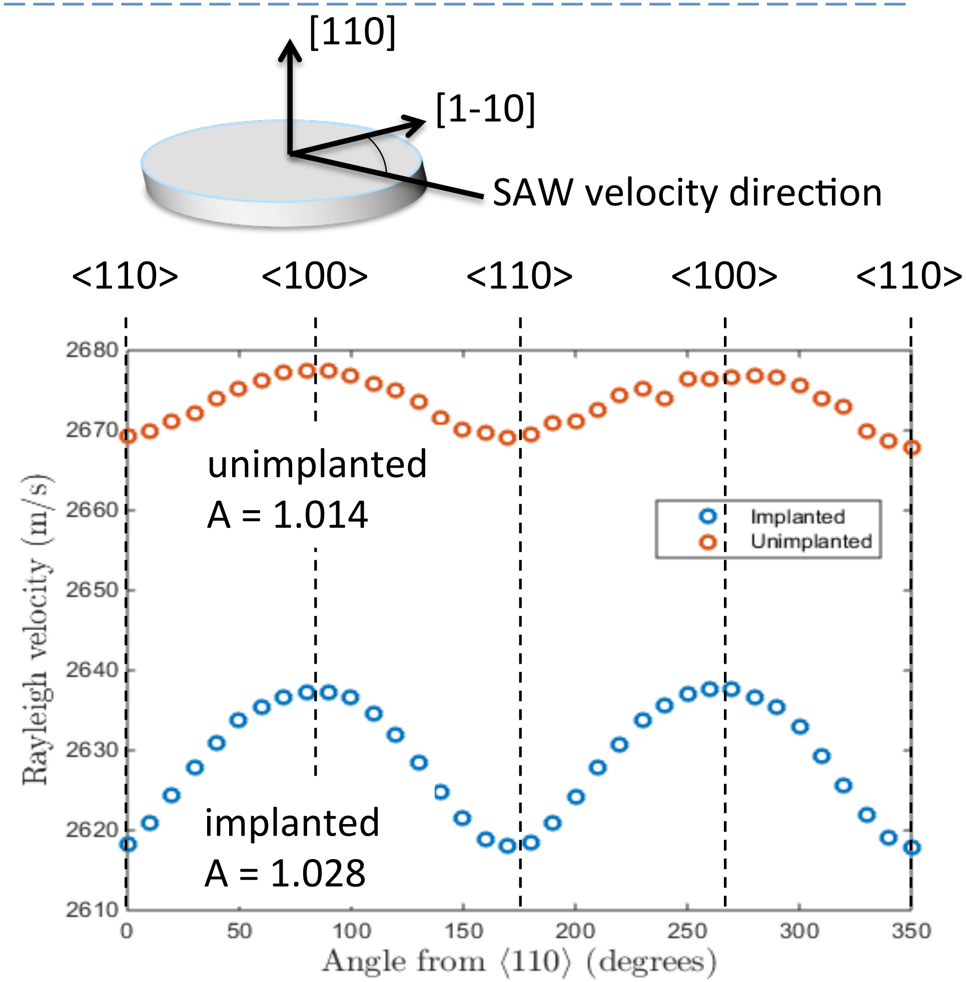

Duncan et al. Applied Physics Letters 109 (15), 151906

[1]Every et al., Ultrasonics (2016)

Thermal Transport Changes

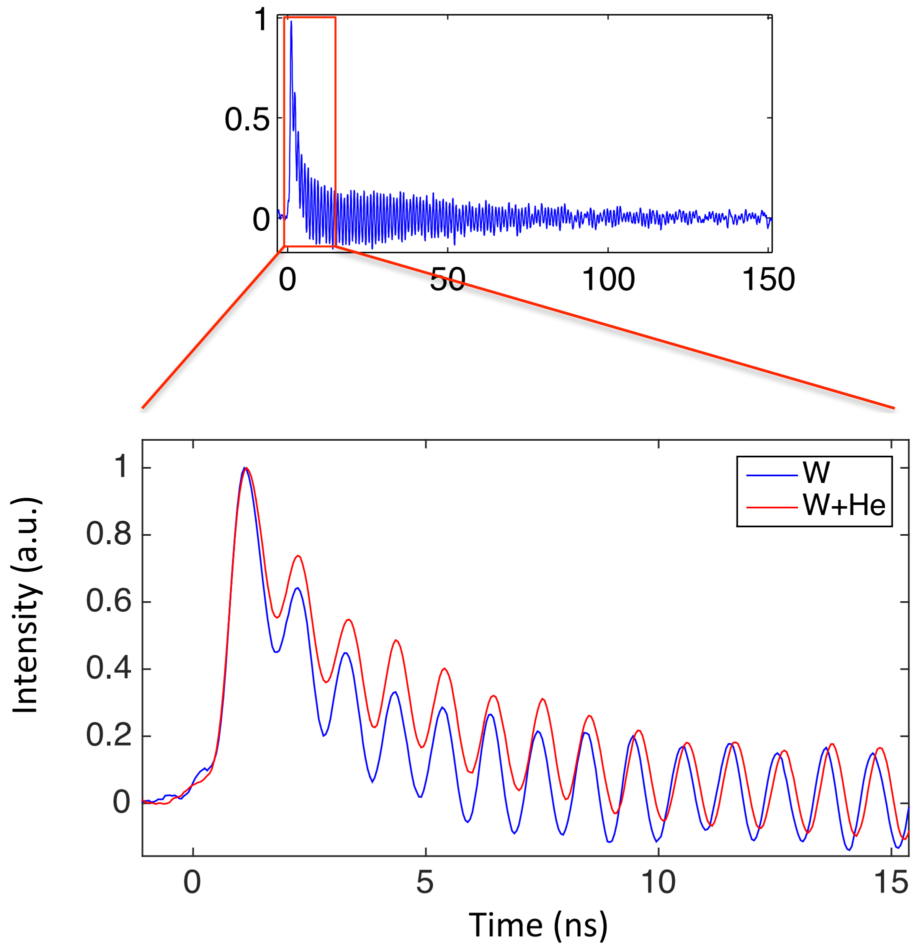

Hofmann et al. Scientific Reports 16042 (2015)

- Transient grating background signal related to decay of thermal grating
- Can fit this to extract thermal diffusivity of ion-implanted layer:

grating decay

$$I = A\mathrm{erfc}\left(q\sqrt{\alpha t}\right) + C\sin(2\pi f t + E)\exp\left(-\frac{t}{F}\right) + G.$$

- Probed depth ~ λ/π

Can measure the thermal diffusivity of ion-implanted layer!
(without modifying sample surface)

Thermal Transport Changes -> Re Effect

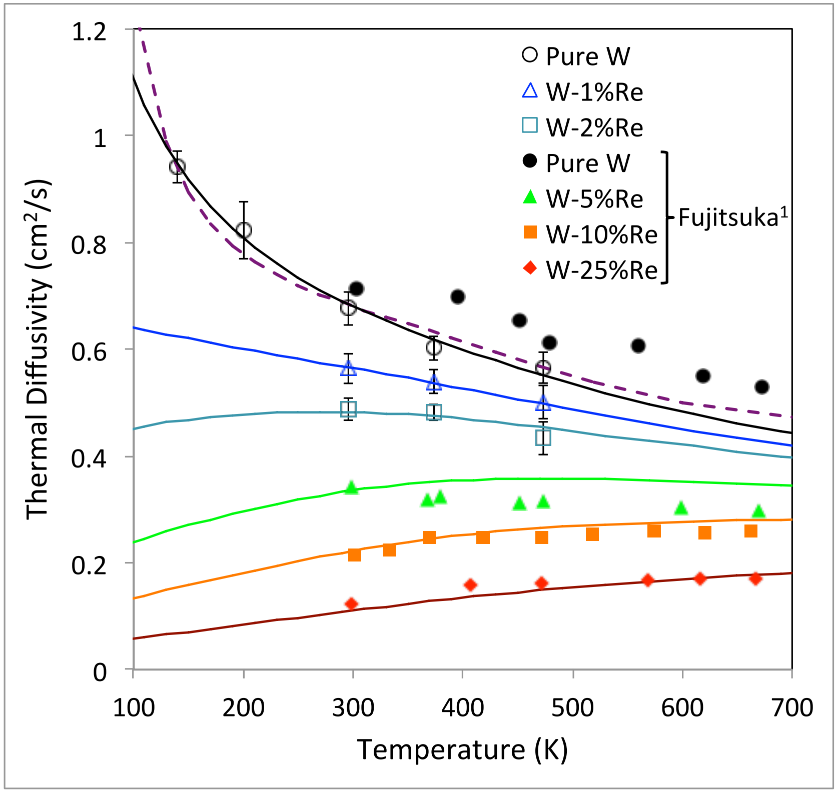

- Good agreement of pure W with literature data
- Reliable extraction of thermal transport parameters by TG
- Clearly see a saturation effect with increasing Re content

Degradation of thermal transport due to transmutation alloying will be important (in DEMO armour 3% of Re will appear within 5 years)[2]

Hofmann et al. Scientific Reports 16042 (2015)

[1]Fujitsuka, M., Journal of Nuclear Materials 283–287 (2000)
[2]Gilbert et al., Nucl. Fusion 52 (2012)

Thermal Transport Changes

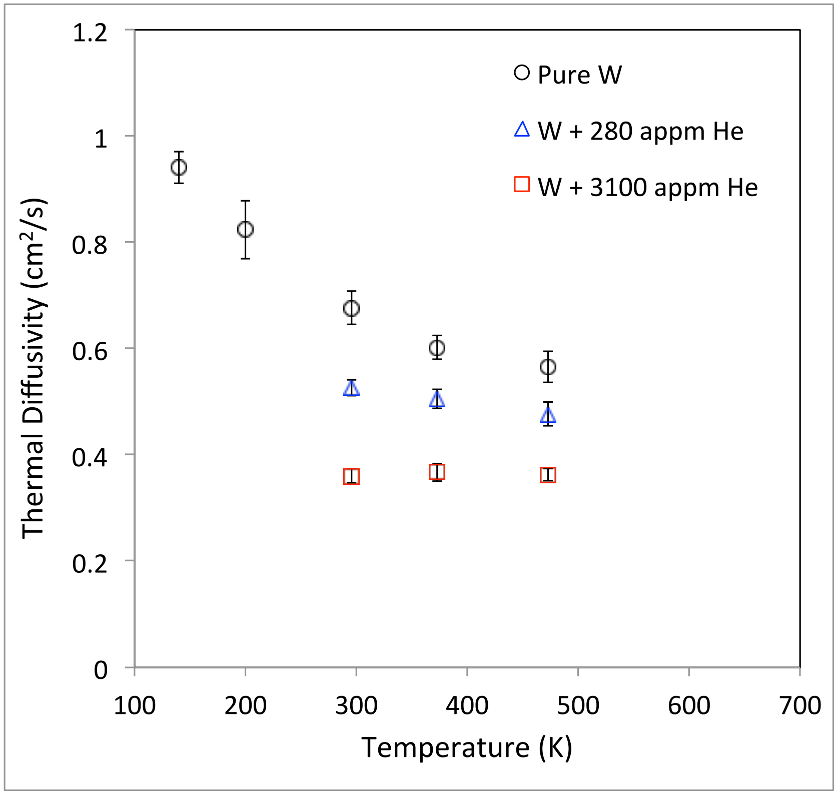

- W + 0.03 at.% helium and W + 0.3 at% helium.
- 0.3 at.% helium reduces RT thermal diffusivity by 50%.

Helium implantation defects have a dramatic effect on thermal diffusivity

How can we predict these changes?

Hofmann et al. Scientific Reports 16042 (2015)

Thermal Transport Changes

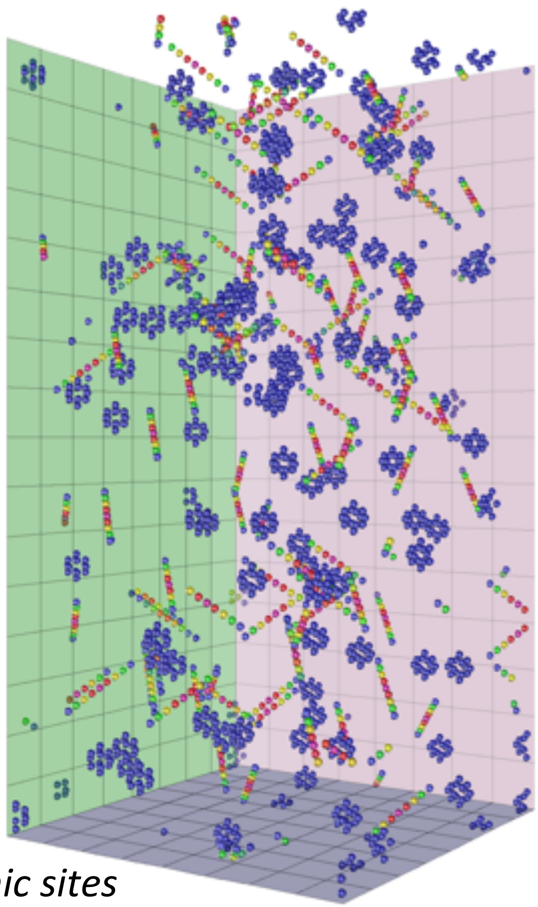

Atomic sites
coloured by scattering rate

Hofmann et al. Scientific Reports 16042 (2015)

- Use Ackland-Thetford EAM potential for tungsten[1], generate defect structure, relax
- Correlate atomic energy in excess of thermal average with scattering rate[2]
  - ➢ Calibrated based on vacancy and self-interstitial electrical resistivity
- Vacancies now appear as "cages" of 8 scattering atoms
- Self interstitials appear as a "string" of atoms with different scattering strength
- Compute electronic scattering rate by summing over all atomic sites

In principle conductivity for any kind of damage structure could be calculated…

[1]Ackland, Thetford, Philos. Mag. A 56 (1987).
[2]Mason, D. R. Journal of Physics: Condensed Matter 27, (2015).

felix.hofmann@eng.ox.ac.uk

Thermal Transport Changes

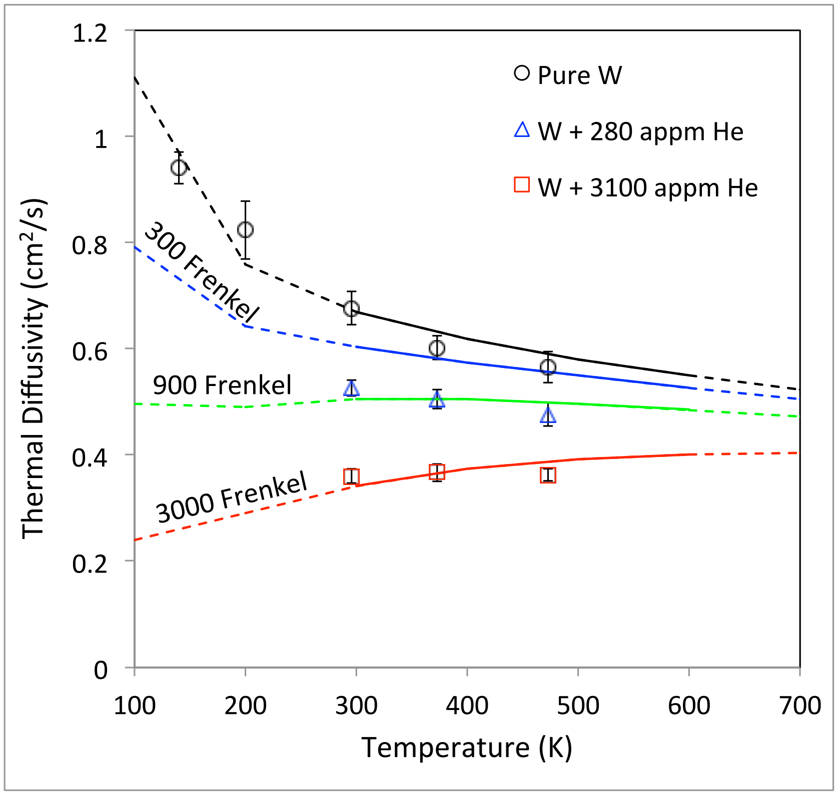

- Predict lower thermal diffusivities for He-implanted samples:
  - 300 appm He -> 900 appm Frenkel defects
  - 3000 appm He -> 3000 appm Frenkel defects
- Decrease of Frenkel:He ratio with increasing dose consistent with OKMC calculations[1]
- At low doses impurities dominate Frenkel defect retention
- At high doses helium dominates Frenkel defect retention

Hofmann et al. Scientific Reports 16042 (2015)

[1] Becquart, C. S. & Domain, C. Journal of Nuclear Materials 385, (2009).

Defect Migration at Higher Temperatures

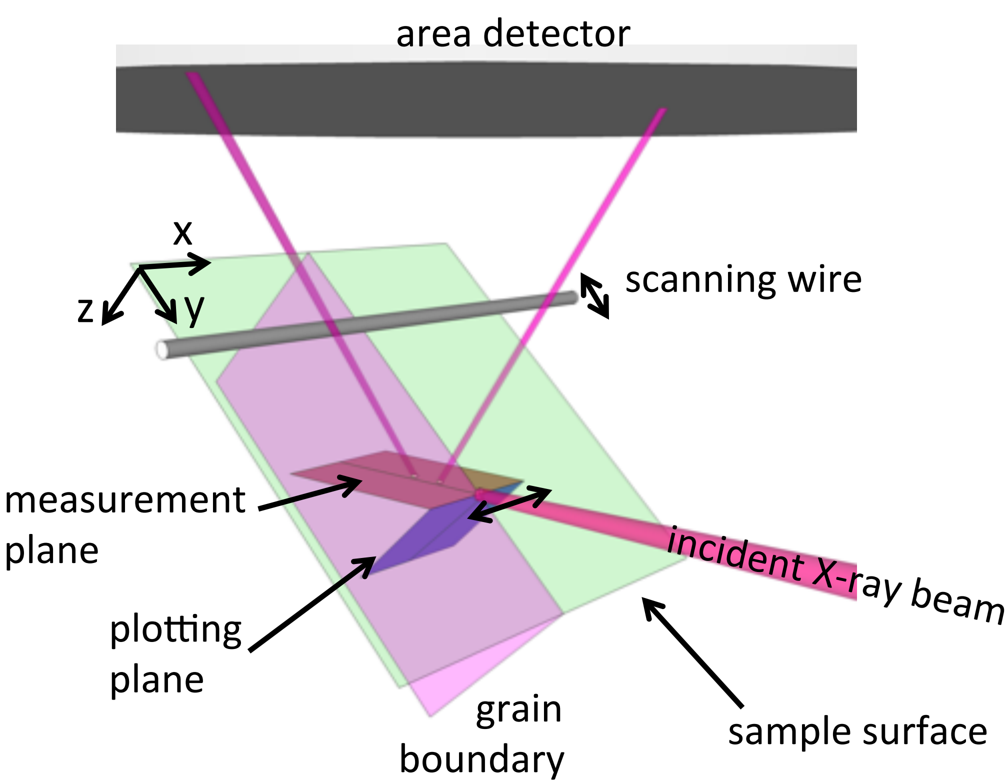

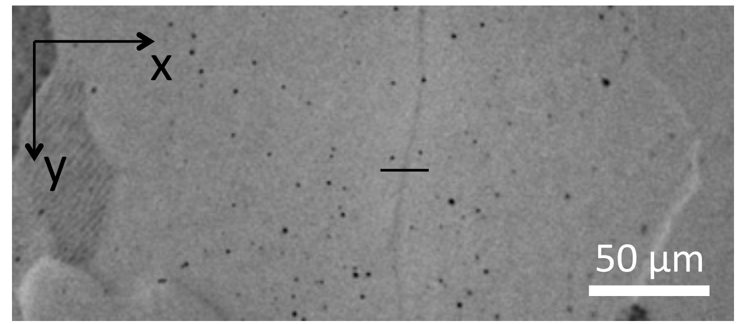

- High purity W, 1673 K anneal, 3000 appm He @ 298K
- Heat treatments:
  - as implanted
  - 1273 K for 12 h
  - 1473 K for 12 h
- Measure deviatoric strain maps in vicinity of grain boundaries

de Broglie et al. Scripta Mater. 107 (2015)

Defect Migration at Higher Temperatures

As-implanted sample e^*_{zz} strain:

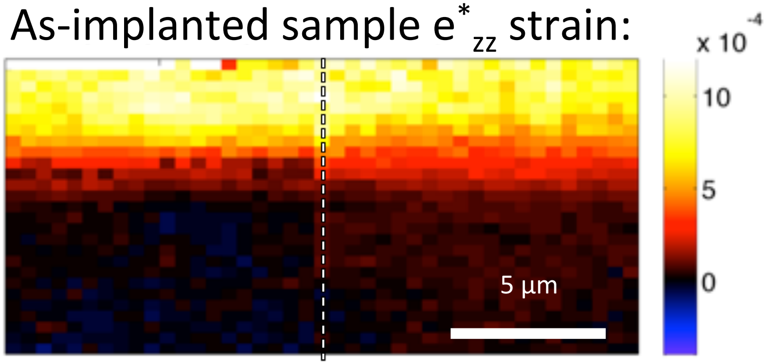

Post-implantation heat treated, 1273 K for 12 hrs, e^*_{zz} strain:

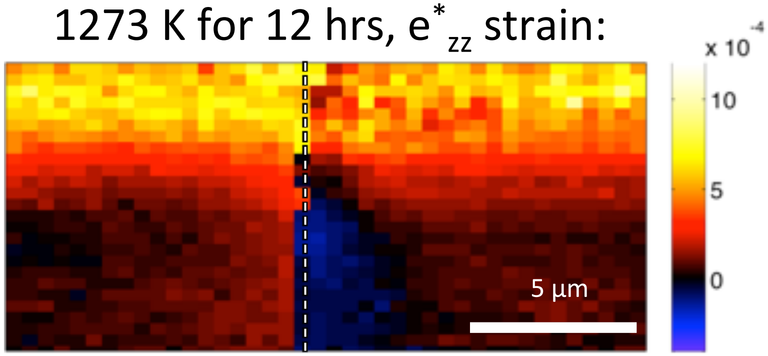

de Broglie et al. Scripta Mater. 107 (2015)

- As-implanted
  - High strain in implanted layer
  - Uniform strain distribution perpendicular to boundary
- After heat treatment:
  - Reduction in out-of plane strain.
  - Inhomogeneous strains appear at grain boundaries

How can these strains be interpreted in terms of lattice swelling?

-> Eigenstrain modelling

Defect Migration at Higher Temperatures

Reconstructed maps of lattice swelling (x 10^{-6})

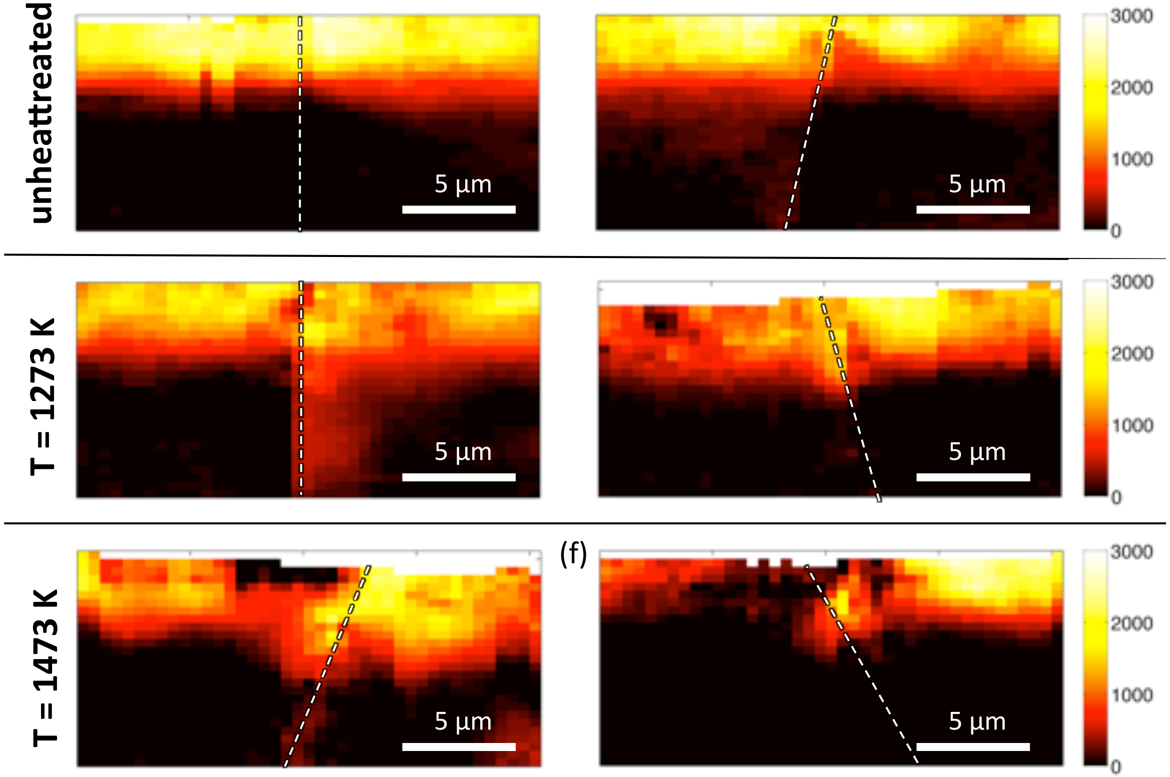

- Swelling confined to implanted layer in as-implanted samples
- Increased heterogeneity after heat treatment
- Reduction in swelling appears grain-orientation dependent
- Some grain boundaries show increased lattice swelling

➢ **Some implantation-induced defects migrate beyond implanted layer!**

de Broglie et al. Scripta Mater. 107 (2015)

Helium-Damage Effect on Deformation

<u>Unimplanted reference</u>

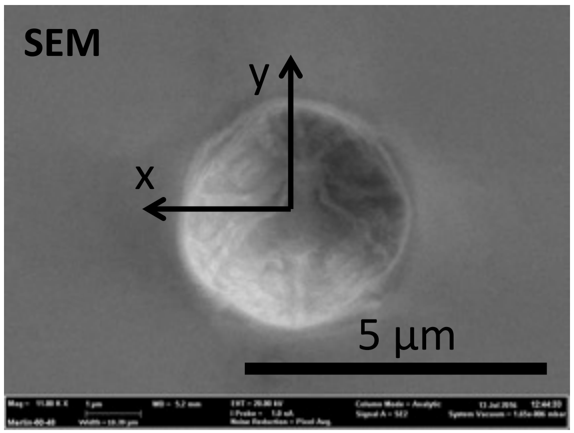

Laue: ε_{zz} deviatoric strain

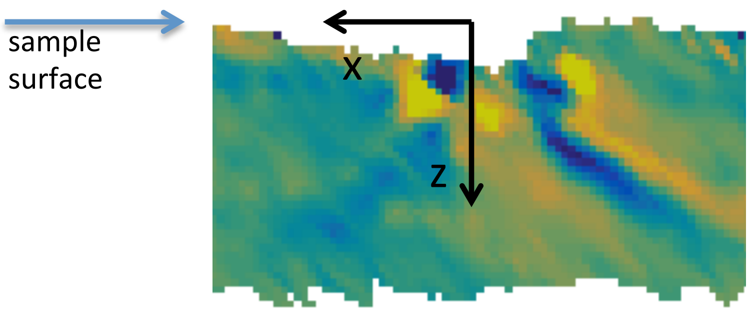

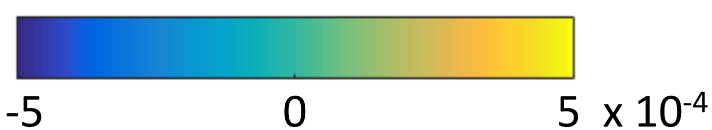

<u>0.3 at% helium-implanted sample</u>

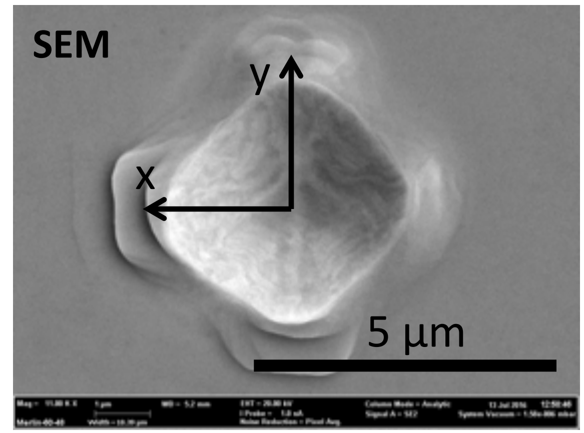

Laue: ε_{zz} deviatoric strain

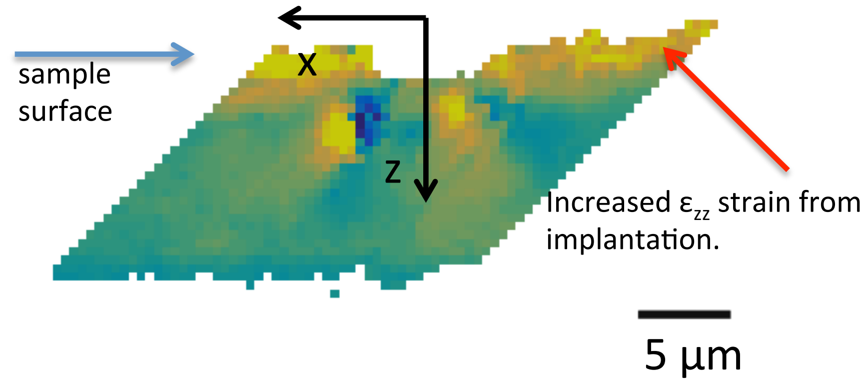

Outline

- Introduction
- Point Defects

  Irradiation-Induced Defects, Lattice Swelling, Modulus Change, Thermal Transport, DFT, MD, Defect Evolution, Interaction with Dislocations

- Ion-Machining Damage

  Coherent X-ray Diffraction Imaging, Nano-scale Lattice Strains and Crystal Defects

- Conclusions

FIB: A Transformational Tool for Nano-Science

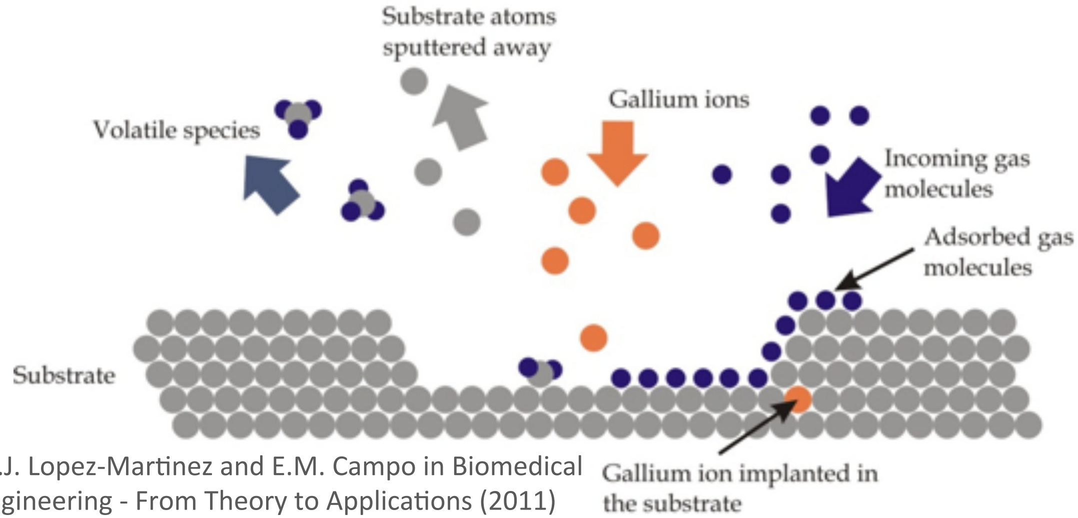

M.J. Lopez-Martinez and E.M. Campo in Biomedical Engineering - From Theory to Applications (2011)

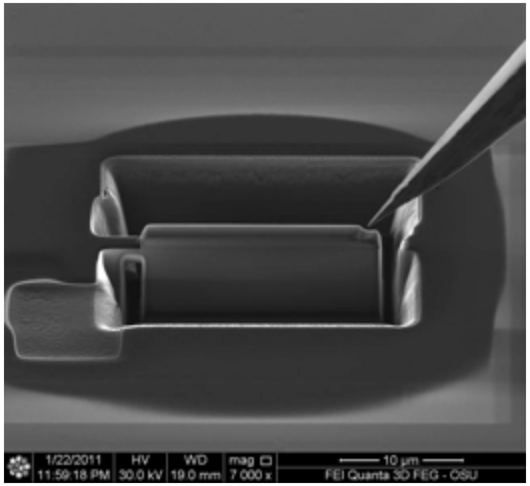

Oregon State University, EM facilities (2011)

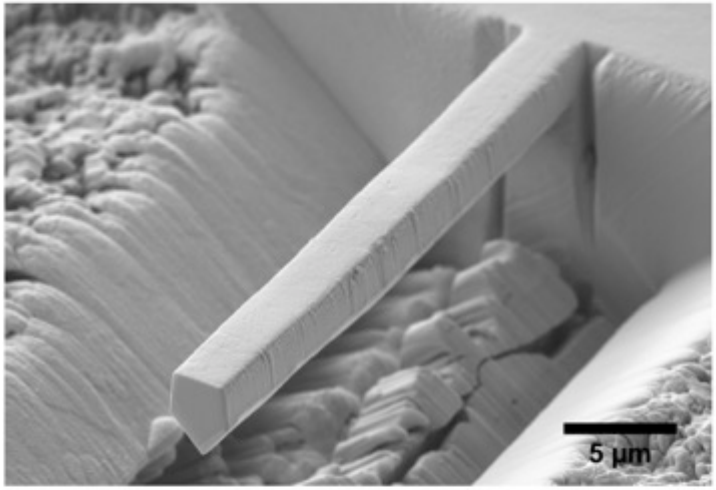

Gibson, DPhil thesis, Oxford (2015)

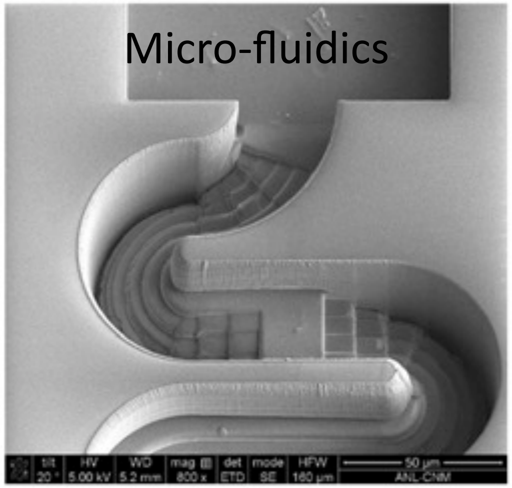

Ocola et al. J. Vac. Sci. Technol. B 31 (2013)

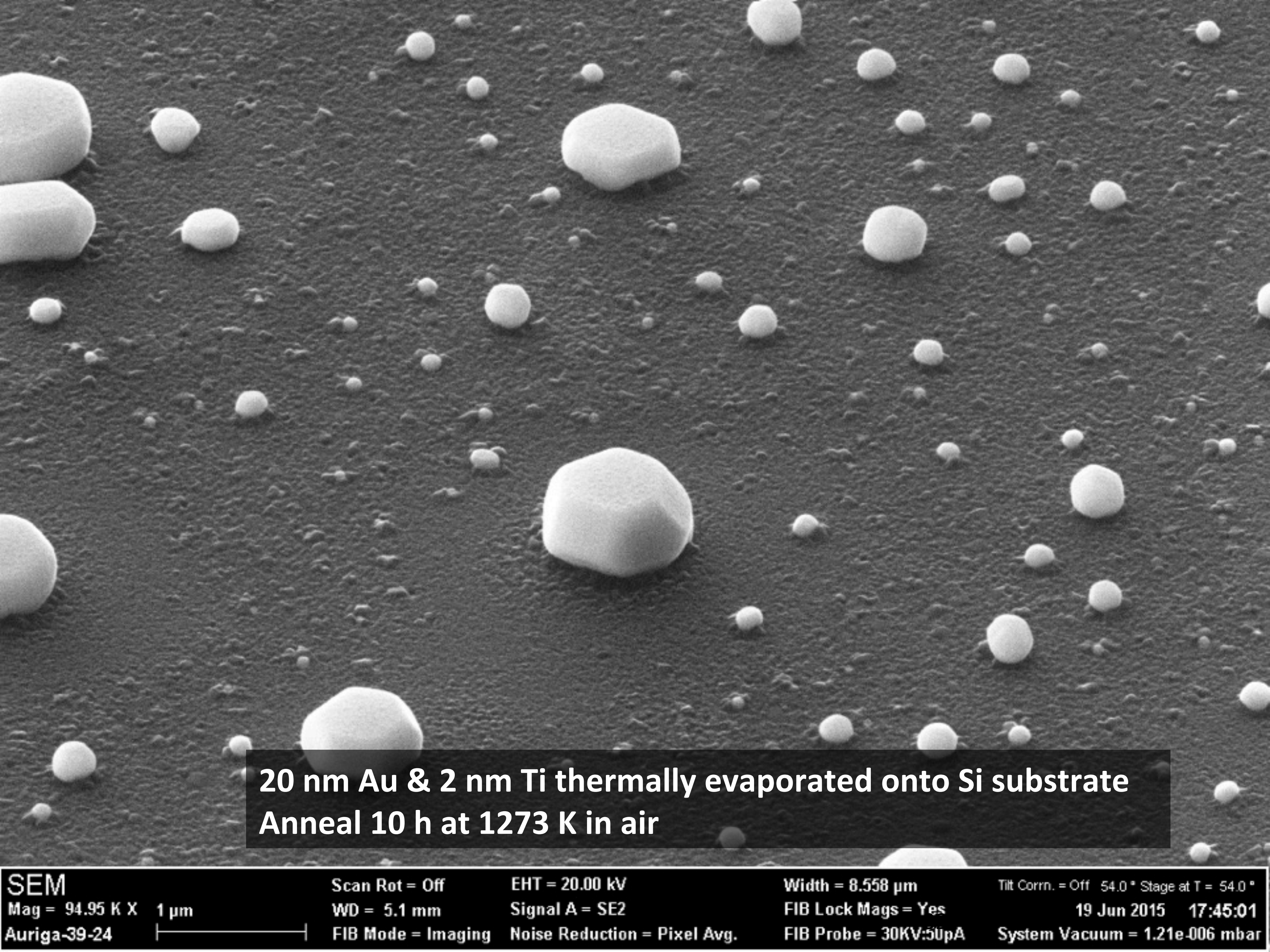
20 nm Au & 2 nm Ti thermally evaporated onto Si substrate
Anneal 10 h at 1273 K in air
SEM
Mag = 94.95 K X
1 µm
Auriga-39-24
Scan Rot = Off
WD = 5.1 mm
FIB Mode = Imaging
EHT = 20.00 kV
Signal A = SE2
Noise Reduction = Pixel Avg.
Width = 8.558 µm
FIB Lock Mags = Yes
FIB Probe = 30KV:50pA
Tilt Corrn. = Off 54.0 ° Stage at T = 54.0 °
19 Jun 2015 17:45:01
System Vacuum = 1.21e-006 mbar

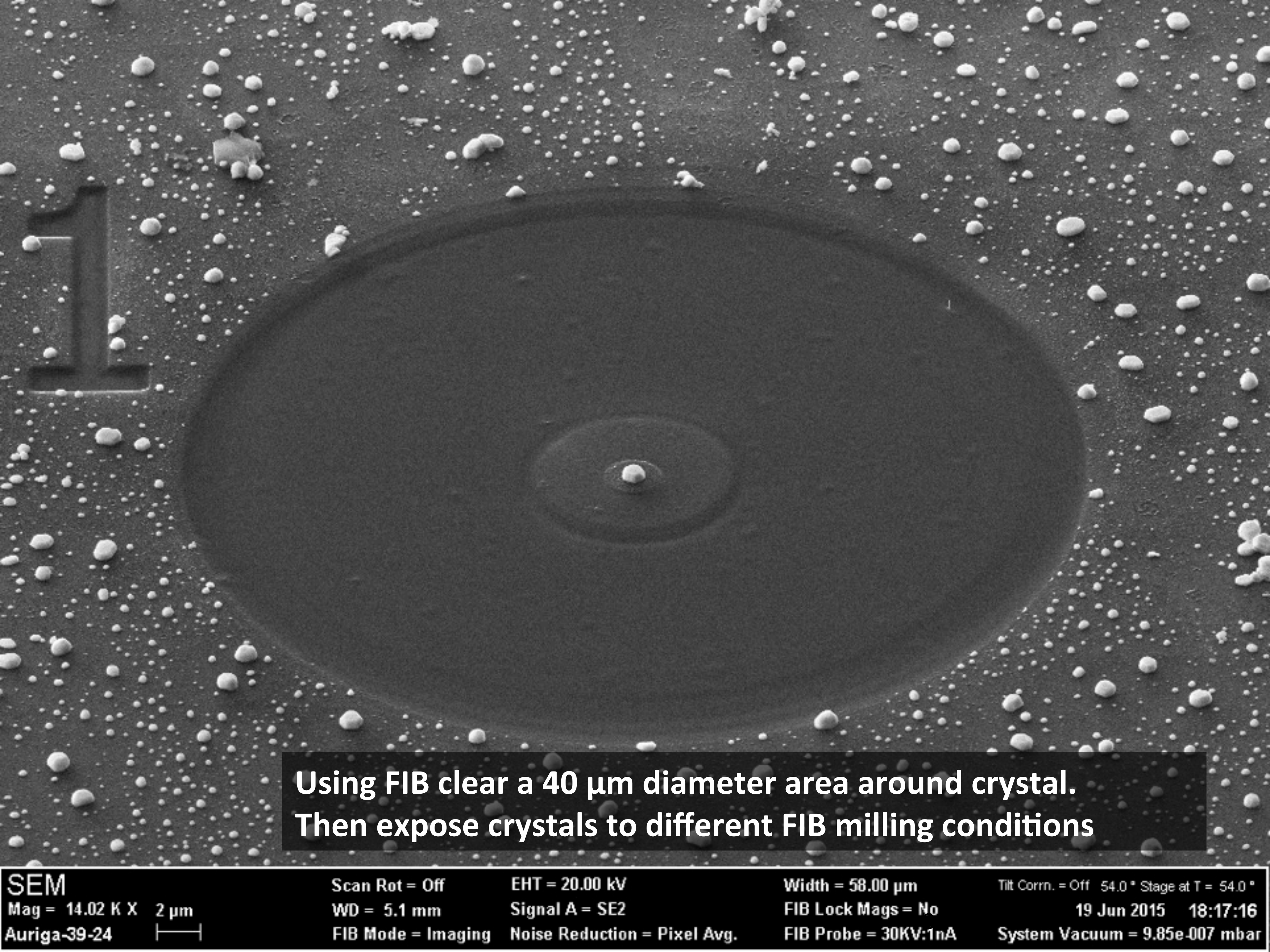
Using FIB clear a 40 µm diameter area around crystal.
Then expose crystals to different FIB milling conditions
1
SEM
Mag = 14.02 K X
2 µm
Auriga-39-24
Scan Rot = Off
WD = 5.1 mm
FIB Mode = Imaging
EHT = 20.00 kV
Signal A = SE2
Noise Reduction = Pixel Avg.
Width = 58.00 µm
FIB Lock Mags = No
FIB Probe = 30KV:1nA
Tilt Corrn. = Off 54.0 ° Stage at T = 54.0 °
19 Jun 2015 18:17:16
System Vacuum = 9.85e-007 mbar

Bragg Coherent Diffraction Imaging

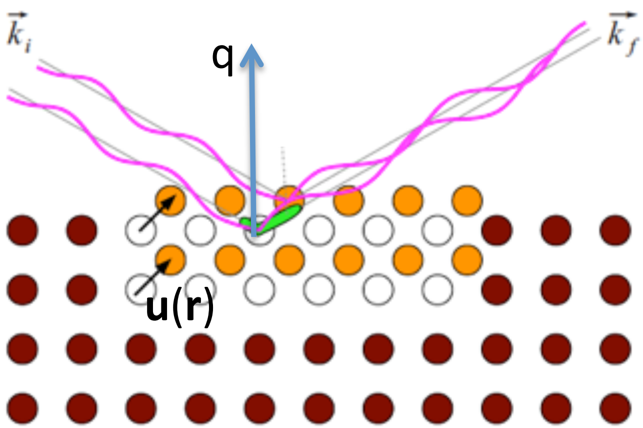

from Newton et al. PRB 82 (2010)

$$\mathbf{q} = \mathbf{k}_f - \mathbf{k}_i$$

scattering vector **q**

Frauenhofer far field diffraction approximation

$$I(\mathbf{q}) \propto \left| \int_0^\infty \underbrace{\rho(\mathbf{r}) s(\mathbf{r}) e^{i\mathbf{q}.\mathbf{u}(\mathbf{r})}}_{\text{Complex electron density}} e^{i\mathbf{q}.\mathbf{r}}\, d\mathbf{r} \right|^2$$

$$I(\mathbf{q}) \propto \left| FT\left[\rho(\mathbf{r}) s(\mathbf{r}) \measuredangle(\mathbf{q}.\mathbf{u}(\mathbf{r}))\right] \right|^2$$

electron density

crystal shape

$\psi(\mathbf{r}) = \mathbf{q}.\mathbf{u}(\mathbf{r})$

"phase"

-> proportional to lattice displacement along **q**!

BCDI Imaging of Crystal Shape and Strain

3D coherent diffraction pattern

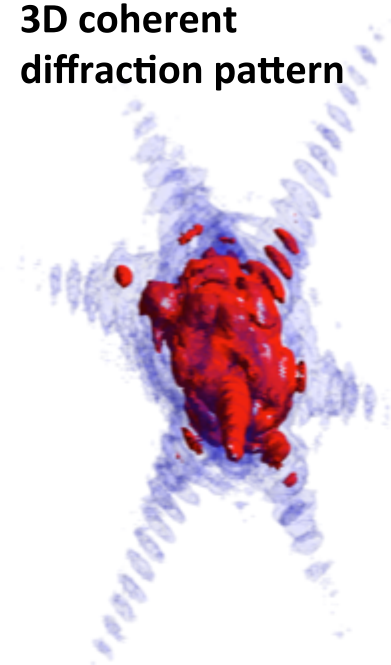

FFT^{-1}

Iterate between real and reciprocal space to retrieve lost phase information

FFT

Reconstructed complex electron density

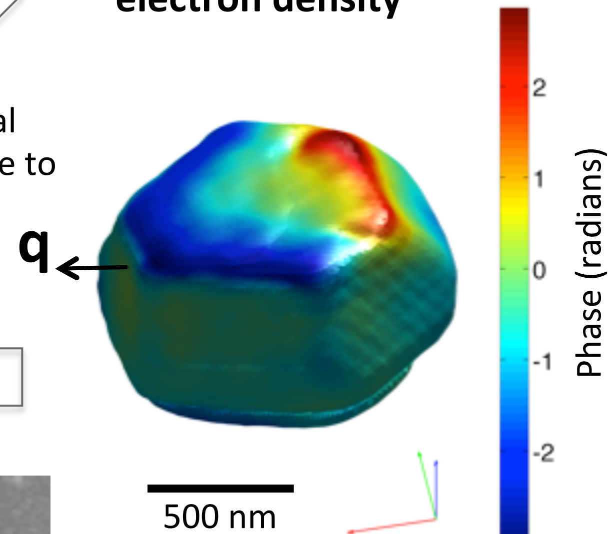

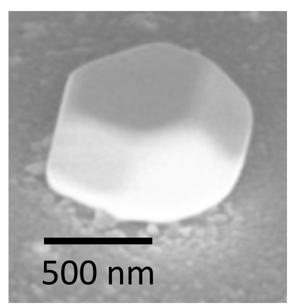

<u>Reciprocal Space Constraint:</u>
Measured intensity of 3D coherent diffraction pattern

<u>Real Space Constraint:</u>
Finite size of object smaller than illuminating coherent beam

Each reflection provides crystal morphology and a projection of the lattice displacement vector along the q vector of that reflection.

felix.hofmann@eng.ox.ac.uk

Many Reflections from the Same Crystal…

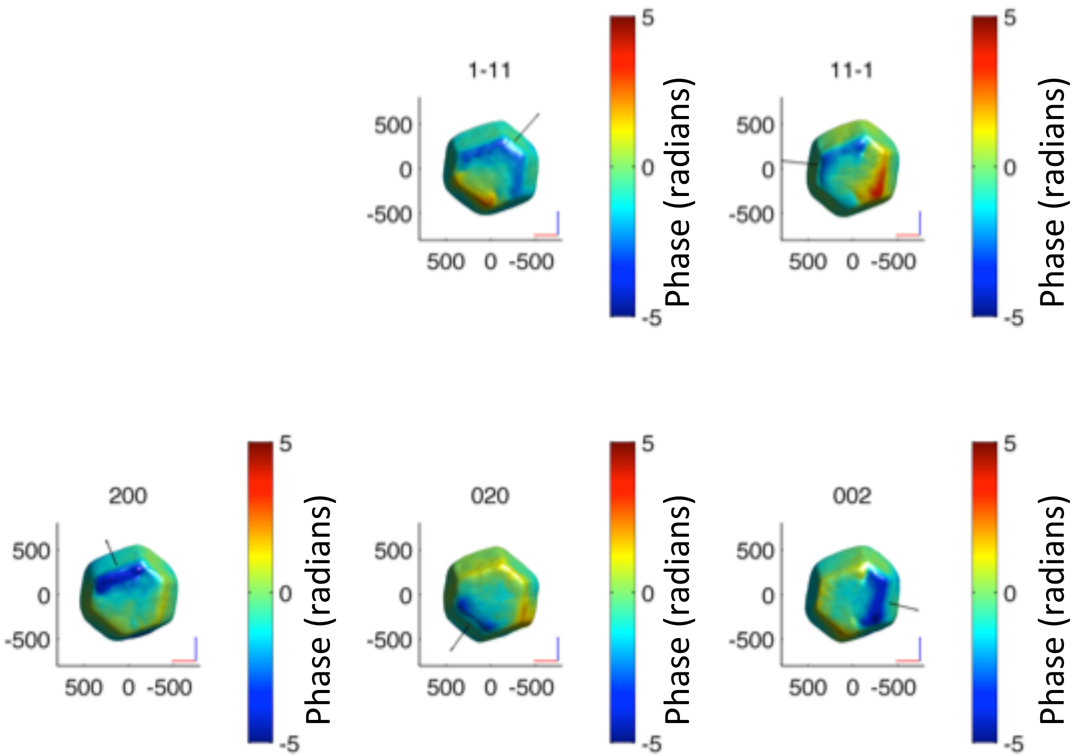

Write out system of equations:

$$\begin{bmatrix} \psi_{1-11}(\mathbf{r}) \\ \psi_{11-1}(\mathbf{r}) \\ \psi_{200}(\mathbf{r}) \\ \psi_{020}(\mathbf{r}) \\ \psi_{002}(\mathbf{r}) \end{bmatrix} = \begin{bmatrix} [\quad \boldsymbol{q}_{1-11} \quad] \\ [\quad \boldsymbol{q}_{11-1} \quad] \\ [\quad \boldsymbol{q}_{200} \quad] \\ [\quad \boldsymbol{q}_{020} \quad] \\ [\quad \boldsymbol{q}_{002} \quad] \end{bmatrix} \begin{bmatrix} \boldsymbol{u}_x(\mathbf{r}) \\ \boldsymbol{u}_y(\mathbf{r}) \\ \boldsymbol{u}_z(\mathbf{r}) \end{bmatrix}$$

Solve for displacement field **u**(r)

Differentiate to calculate strain

Multiply by stiffness to get stress, etc.

Can reconstruct the full, 3D-resolved lattice strain tensor!

Low Dose FIB Imaging

BCDI reconstructed morphology

1 µm

Scanning electron micrograph

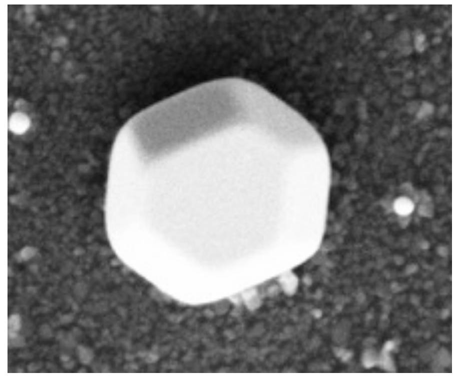

Typical low dose FIB image of gold crystals vs SEM

gold crystal!

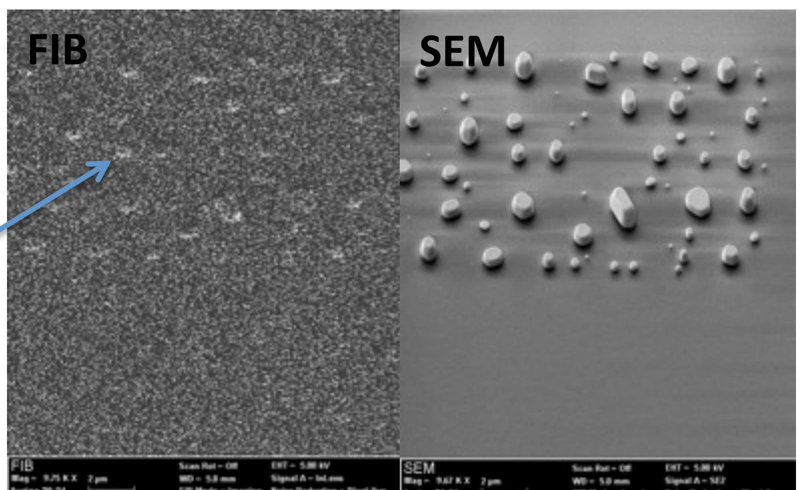

FIB imaging conditions:

- 30 keV Ga^+
- 50 pA
- 4.2×10^4 ions/ μm^2 (scan speed 1)

This causes (SRIM calculation):

- ~20 nm thick damaged layer
- max. ~0.025 dpa
- max. ~45 appm Ga
- Negligible Au removal by sputtering

Low Dose FIB Imaging -> Experimental Strains

Total lattice displacement; measured reflections

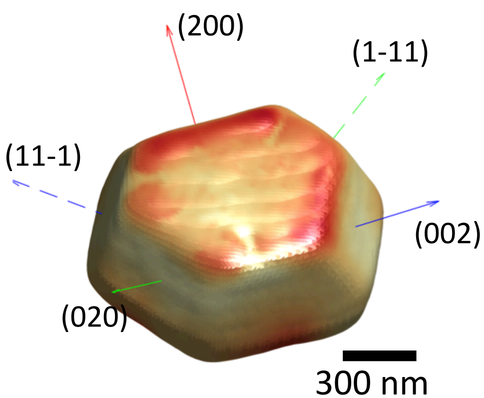

Strain coordinates

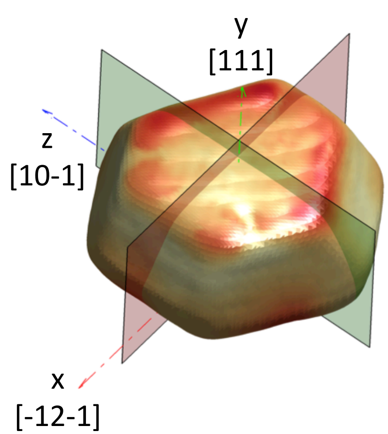

Strain tensor in xy plane (red)

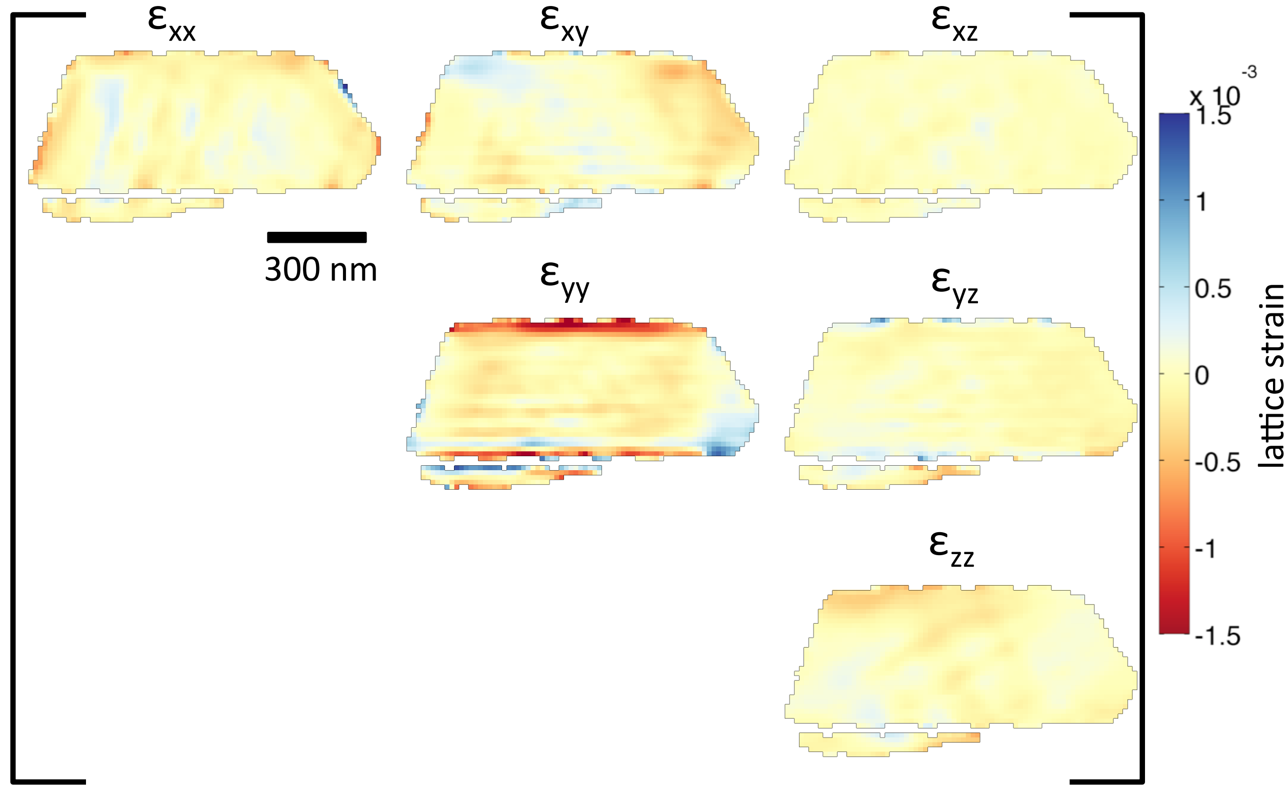

- Full 3D-resolved strain tensor (uncertainty ~10^{-4})
- Large negative strain near implanted surface -> **Lattice contraction?**
- **How can this be modelled?**

Low Dose FIB Imaging -> Modelling

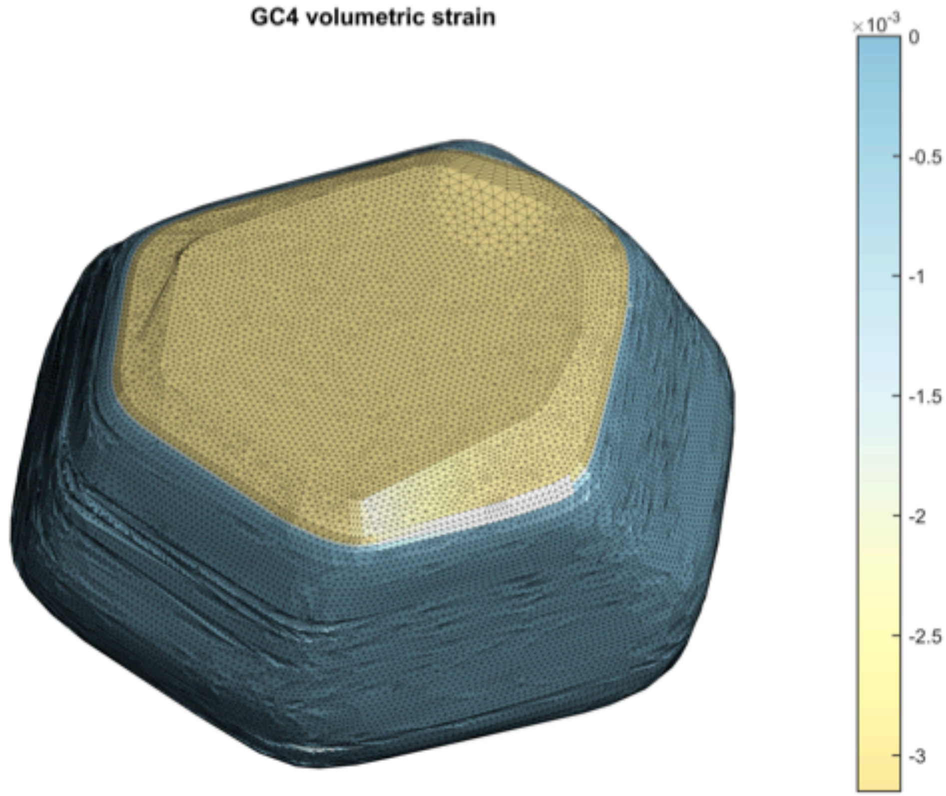

Apply a volumetric Eigenstrain to the top, implanted layer.

Solve for strains inside the crystal using anisotropic elasticity.

felix.hofmann@eng.ox.ac.uk

Low Dose FIB Imaging

Experimental strain tensor in xy plane (red)

Calculated strain tensor in xy plane (red)

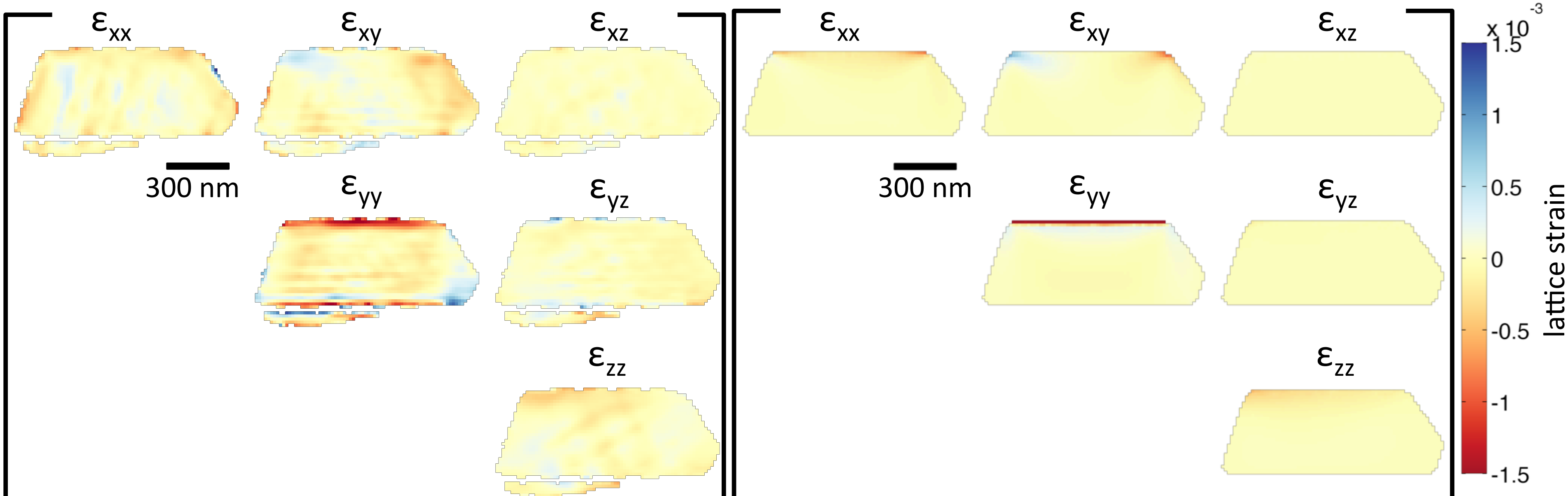

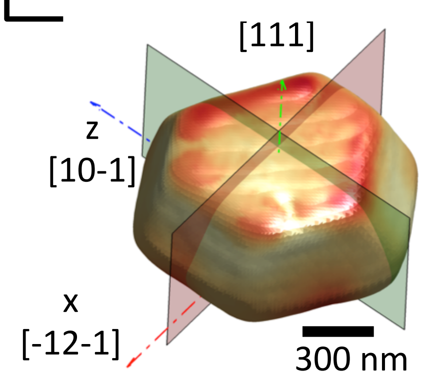

- Excellent agreement of FE model and experiment
- Spurious experimental strains on lower crystal surface
- FIB imaging causes volumetric lattice strain $\varepsilon_v = -3.15 \times 10^{-3}$
  -> Lattice contraction

How can this be explained?

Crystal A: Lattice Contraction Analysis

- Lattice swelling: $\varepsilon_v = \sum_A n_A \Omega_r^{(A)}$
- Relaxation volumes for Vacancies and SIAs in gold:
  Literature: $\Omega_r(V) = -0.27\ \Omega_0$[1]; $\Omega_r(SIA) = 1.5\ \Omega_0$[2];
  Our DFT: $\Omega_r(V) = -0.38\ \Omega_0$; $\Omega_r(SIA) = 2.0\ \Omega_0$;
- Lattice contraction -> Vacancy dominated -> SIAs escape to surface and form adatoms
  Free surface plays central role in determining damage retained
- Lower bound vacancy concentration estimate:
  -> 7.5 x 10-3 at. fraction, i.e. ~200 V per Ga ion are retained
- SRIM upper bound estimate: ~400 Frenkel defects per Ga ion are generated
  (excluding replacement collision)

Even a single FIB image causes large lattice strains.
Our new method allows quantitative analysis of these strains.

[1] Korzhavyi et al. PRB 59 (1999)
[2] Daw et al. Mater. Sci. Rep. 9 (1993)

Higher Fluence FIB Milling

BCDI reconstructed morphology

Scanning electron micrograph

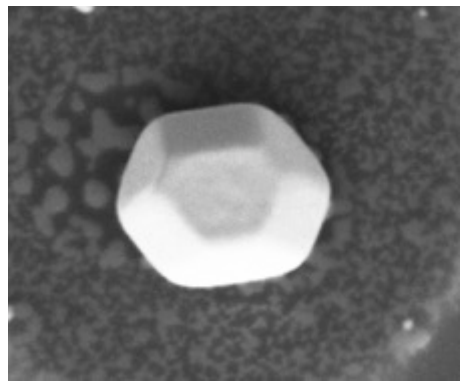

SRIM-predicted damage and Ga concentration

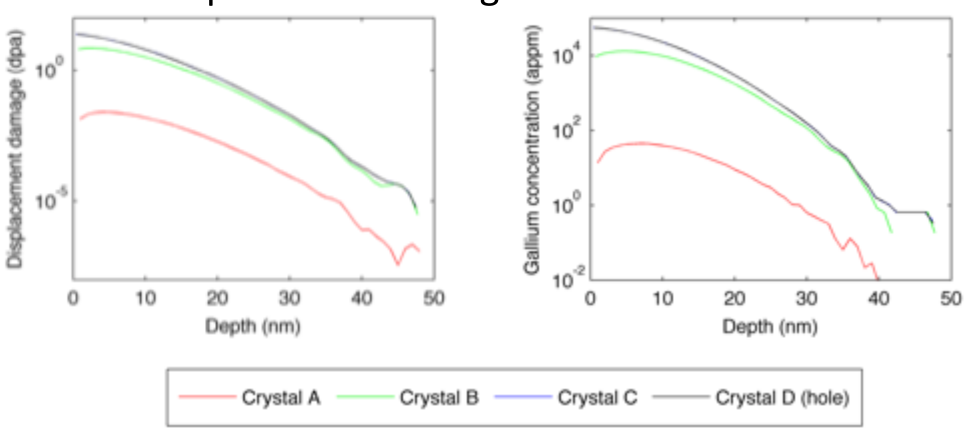

FIB milling conditions:

- 30 keV Ga^+
- 50 pA
- 1.5×10^8 ions/ μm^2

This causes (SRIM calculation):

- ~20 nm thick damaged layer
- max. ~24 dpa
- max. ~0.054 at. fr. Ga
- ~40 nm Au removed by sputtering

Higher Fluence FIB Milling

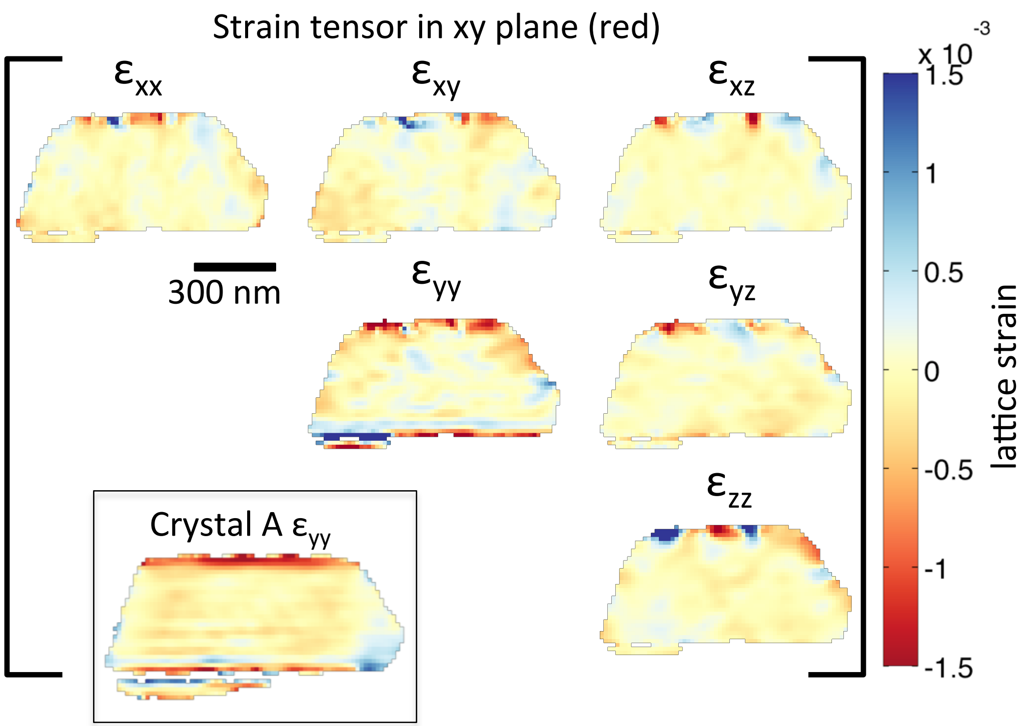

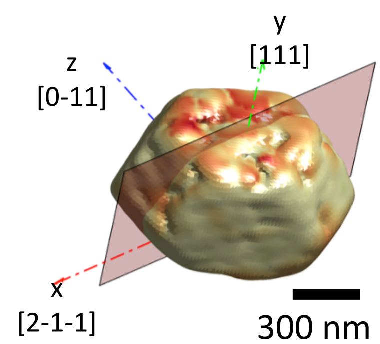

- Non-uniform ε_{yy} strain in implanted layer.
- Large positive and negative strains also in <u>all</u> other strain components.

Very different from crystal A

Higher Fluence FIB Milling -> Larger Defects

Reconstructed crystal C

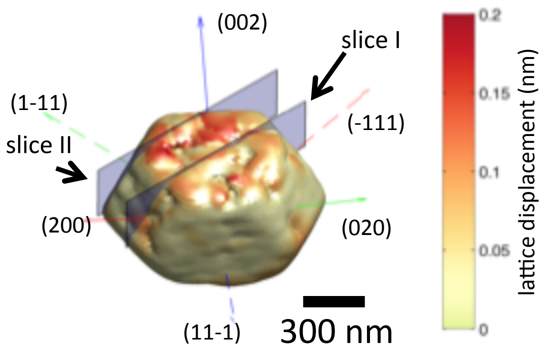

Crystal reflection amplitudes and phases on slice II

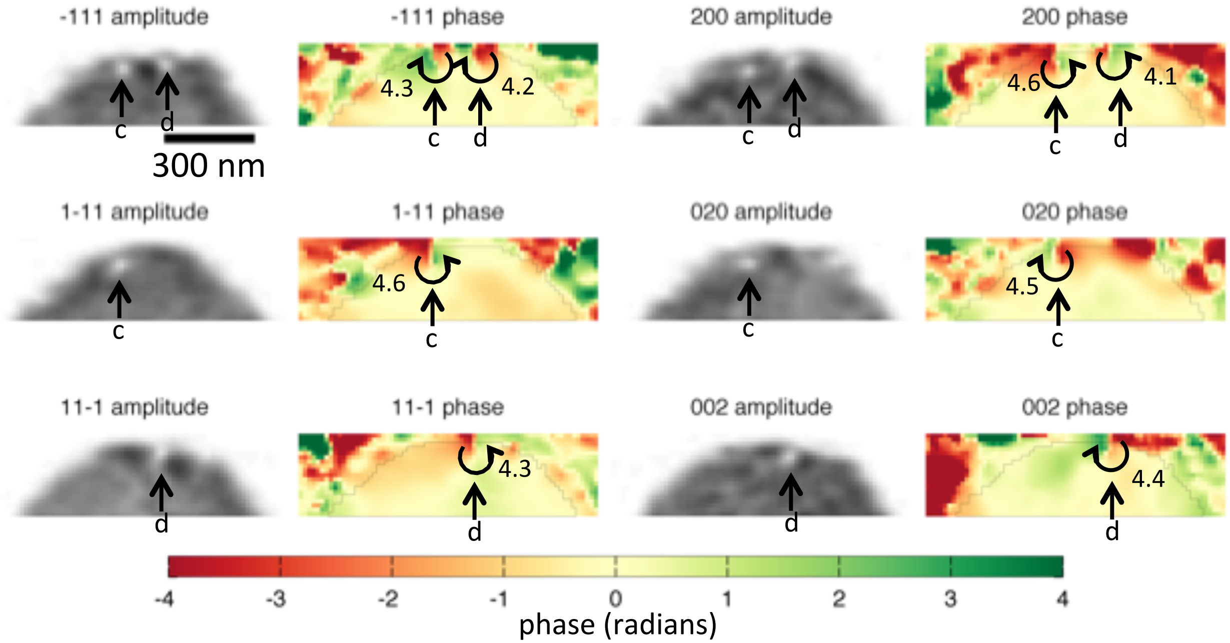

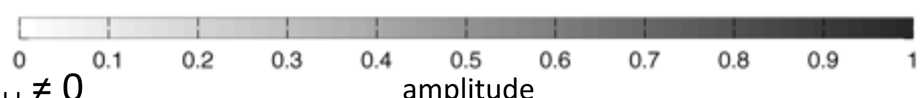

- Dislocation visibility in amplitude: $b.q_{hkl} \neq 0$
- Phase jump in Burgers circuit: $\Delta\psi_{hkl} = b.q_{hkl}$
- Defects are stair-rod dislocations with b = a/3<110>
  -> Formed by interaction of 2 Shockley partials e.g. a/6[21-1]+a/6[-21-1] -> a/3[01-1]
  -> Sessile hence retained?

Higher Fluence FIB Milling -> Dislocation Structure

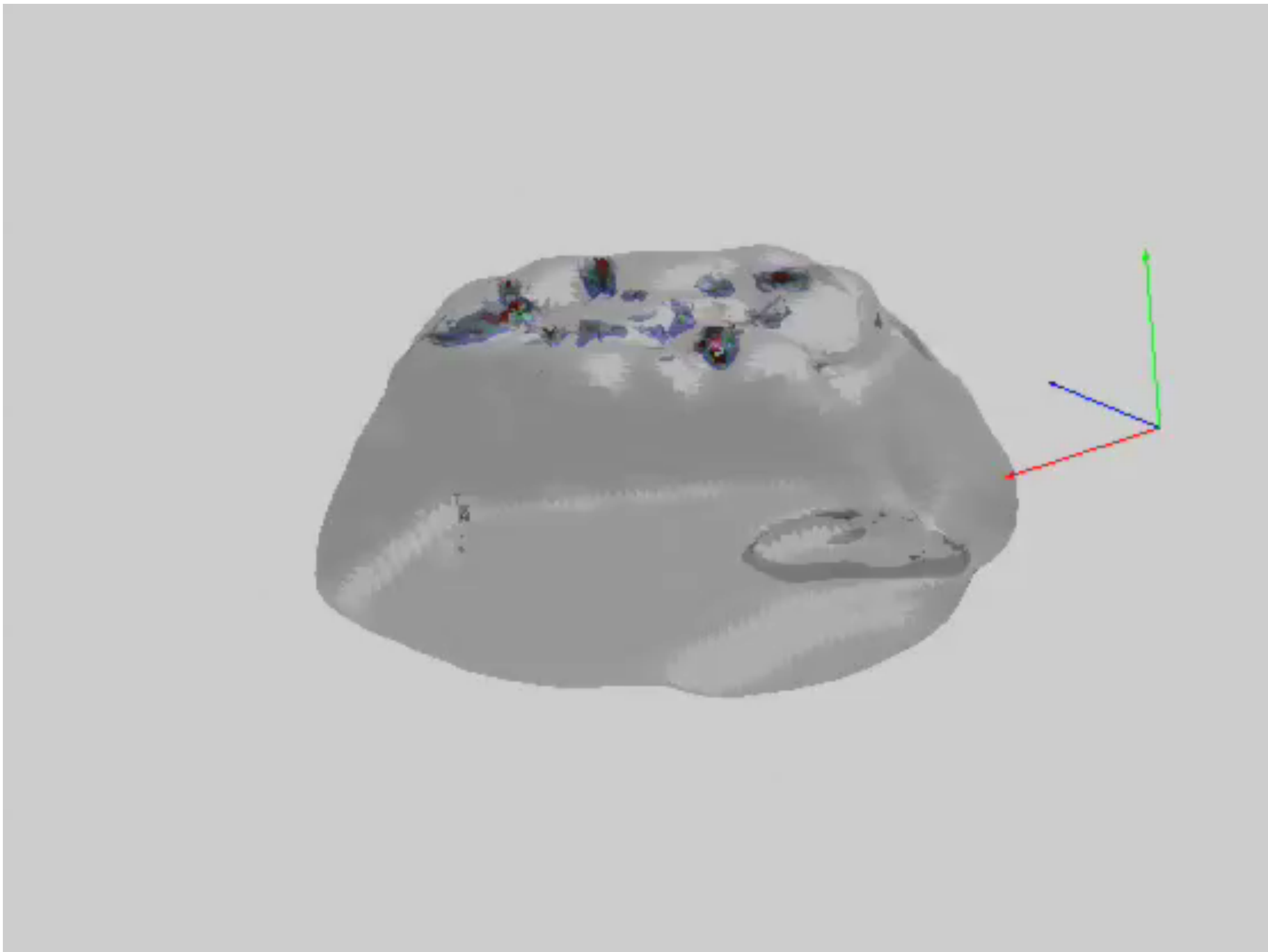

Crystal D: Lattice Strains

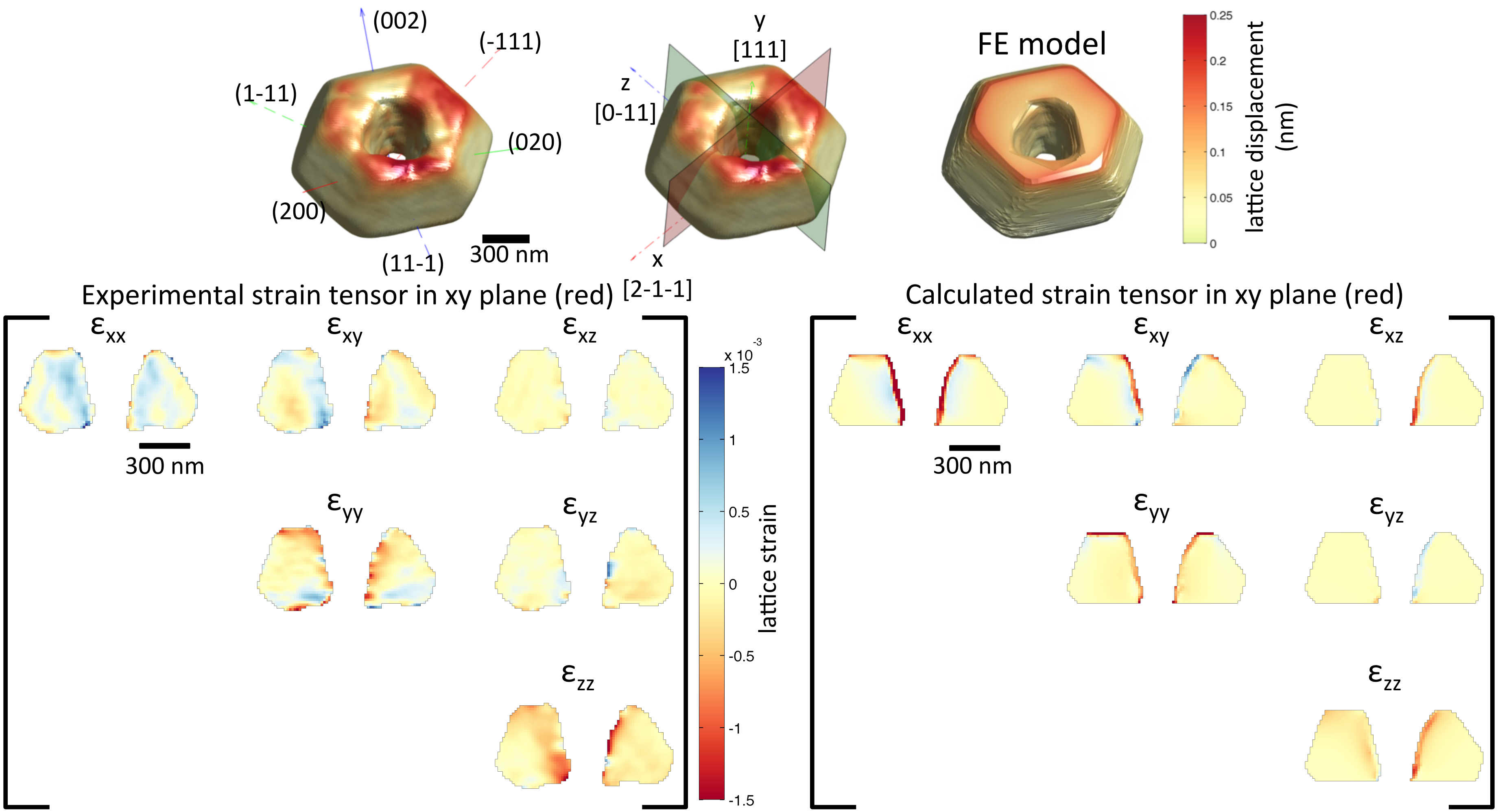

Complex strain fields that extend far beyond the implanted layer thickness…

Conclusions

- Combining multi-technique characterisation can shed light on the complex changes in mechanical and physical material properties crystal lattice defects cause.
- Using multi-scale calculations we can start to form a joined up understanding of these changes.
- Using Coherent X-ray diffraction allows non-destructive 3D nano-scale probing of lattice strains & defects in complex objects.
- FIB-milling provides a fantastic tool for nano-scale machining, but every use introduces damage that must be accounted for.

Converging time and length-scales accessible to experiments and modelling make for a very exciting future!

Acknowledgements

My Group
S. Das
I. deBroglie
H. Yu
M.A. Reza

Micro-mechanics
D.E.J. Armstrong
Y Zayachuk,
C.E. Beck

Modelling
E. Tarleton
P.-W. Ma
D. Nguyen Manh
S.L. Dudarev
D. Mason
M. Gilbert

X-ray experiments
R.J. Harder
W. Liu
R. Xu
N. W. Phillips
B. Abbey
J. N. Clark
I. K. Robinson

Microscopy
Y. Liu

Laser measurements
K.A. Nelson
A. Maznev
R.A. Duncan
J.K. Eliason

Oxford – CCFE – Argonne NL – Brookhaven – MIT – LaTrobe

The Leverhulme Trust

European Research Council
Established by the European Commission

EPSRC

Invisible – RPG-2016-190

AtoFun – StG 714697

MFFP – EP/H018921/1